Characterisation of 3D-printed micro-structures for optics

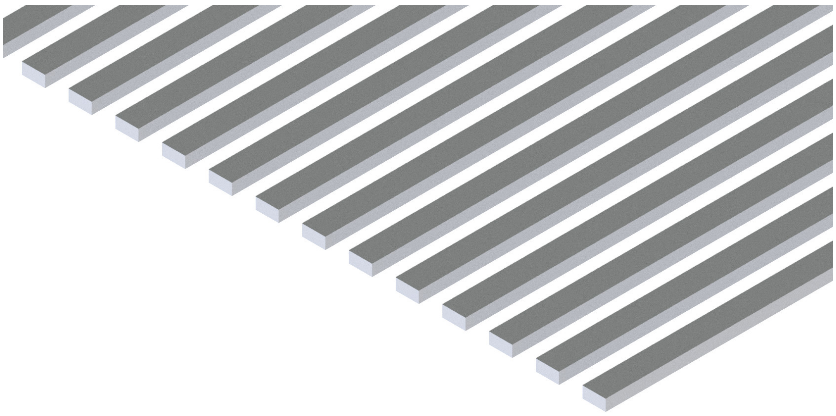

THESIS

submitted in partial fulfillment of the
requirements for the degree of

BACHELOR OF SCIENCE
in
PHYSICS

Author : Evert Stolte
Student ID : 1671871
Supervisor : Martin van Exter
2^{nd} corrector : Daniela Kraft

Leiden, The Netherlands, July 1, 2018

Characterisation of 3D-printed micro-structures for optics

Evert Stolte

Huygens-Kamerlingh Onnes Laboratory, Leiden University
P.O. Box 9500, 2300 RA Leiden, The Netherlands

July 1, 2018

Abstract

This research explores the possibility of producing acrylic micro-structures for optical purposes with a Nanoscribe 3D-printer, which uses two-photon polymerisation. More specifically, it tries to characterise the effect of inherent flaws of the 3D-printing production method on far-field transmission optics. The studied samples are gratings with different periodicities ranging from 4 to 1 μm and samples with flat and tilted surfaces. The gratings show optical effects from variations in displacement, duty-cycle and height, and scattering effects from writing lines. Steps are taken towards 3D-printing multi-grating layer samples, with the end goal of producing a woodpile structure and other multi-layer photonic crystals.

Contents

Chapter 1

Introduction

From early on in optics, it was understood that light didn't consist simply of straight geometric rays, but rather acted as a wave.
Interference and diffraction effects are found when a travelling light wave comes across an obstruction, and the nature of this obstruction can change the incoming wave to a different outgoing wave. A simple example of an obstruction would be the double slit, which changes a plane wave, uniform intensity everywhere, to a wave with a sine-like spatial distribution of amplitude.

Shining light on structures is the main way light has been experimentally researched, and still is. From one-dimensional multi-slits, to two-dimensional reflection gratings, and more recently also extensively 3D structures.[1] From our understanding of light, new structures are invented with more interesting and useful properties like total reflection mirrors, or glass fibre as a wave guide.

The deviation from geometrical optics is only really apparent when the structure is of the scale of the wavelength. For this reason the most interesting structures are made at this wavelength scale. Light in the spectrum visible by humans, and thus the most interesting spectrum, has a wavelength around 600 nm. This has posed technical difficulties in constructing the desired structure. It is only since the end of the 20$^{\text{th}}$ century that production methods for accurate structure on nano scale have become available to researchers.[2] Methods like electron beam lithography have paved the way for the creation of 2D structures on nano scale.[3] [4]

However, constructing in the third dimension proved to be more difficult. For example, cavities are not easily made under a surface with lithography from above. A different kind of manufacturing method was developed. Instead of cutting material away as in lithography, material can be solidified at locations. This is a 3D printing production method, which has been around for more than 30 years for macroscopic structures. One idea to downscale the printing size is a method called two-photon polymerisation, which involves exciting monomers to the polymerisation energy level not with one photon, but with two lower energy photons.

In recent years, a company called Nanoscribe has taken the two-photon polymerisation 3D printing idea and developed it into a product. Their Nanoscribe 3D printer is capable of fabricating structure features smaller than a micron, for simple designs even on the 300 nm scale.[5]

University Leiden has bought a Nanoscribe machine recently in 2016. It has already been used by other physics groups. The Quantum Optics department is now interested in using the machine to create and investigate complex optical 3D structures. For this purpose, it is important to investigate and characterise the limitations and problems of manufacturing objects with the Nanoscribe in an optical context. The effect of nonconformity between intended and produced structure on the optical far field diffraction pattern will be researched, as well as unintended scattering from surface roughness.

A basic structure to explore these properties would be a grating consisting of parallel bars. Other important structures to characterise would be flat surfaces to investigate the effects of surface roughness. More interesting structures would involve multiple layers of gratings.

One optical multi-layer periodic structure that is of particular interest is the 'woodpile' crystal: Layers of parallel bars on top of each other, turned 90° every other layer like stacked wooden logs. This structure has been made and researched in the past, because of it's optical band gap properties and relatively simple manufacture method of stacking thin bars.[6] The wood pile has also been produced with similar photon polymerisation methods and used for multiple purposes.[7][8][9] However, with the Nanoscribe, we see an opportunity to modify this structure. Instead of a 90° difference between layers, a crystal with another angle can be made with the Nanoscribe. This twisted woodpile has different transmissions in right- and left-handed polarised light.[10] The Nanoscribe has been used to print and research optical chiral crystals consisting of helices.[11]

Concluding, the first goal of this research is to characterise the possibilities and limitations of Nanoscribe 3D printed structures for optical purposes, starting with the production of gratings and flat surfaces. And secondly, make steps to produce and research the transmission of optical 3D periodic structures like the twisted woodpile.

Chapter 2

Theory

2.1 Fraunhofer optics

In order to quantify the mistakes in the optical transmission through the 3D printed structure, the transmission wave needs to be compared with how the light pattern would look like when the structure would be ideal. It is therefore crucial to be able to calculate and predict the transmission pattern of samples.

Fraunhofer optics gives us a first and simple tool to analyse the diffraction of an obstruction. The electronic field far behind the plane obstruction is given by the Fourier transform of the so-called aperture field.[12] This field is given by the field inside the aperture of the plane obstruction. The aperture field has both an amplitude and a phase, and is determined by the incoming field and the effects on phase and amplitude by the plane obstruction.

An example of a plane obstruction would be a wall with one straight vertical slit of width b. The incident field is a coherent plane wave with amplitude E_0, phase ϕ_0, and k-vector $k = \frac{2\pi}{\lambda}$. In the obstruction plane, the plane wave would not be changed inside the slit. However outside the slit, the wave would be nullified. This obstruction is described mathematically by the aperture field t. The total field containing incoming field and aperture field would then be given by:

$$E_0 e^{i\phi_0} \cdot t(x) = \begin{cases} E_0 \cdot e^{i\phi_0} & : -\frac{b}{2} < x < \frac{b}{2} \\ 0 & : \text{ elsewhere} \end{cases} \tag{2.1}$$

This is simply a rectangle with an amplitude equal to E_0. This field has spatial frequencies k_x that are, according to Fraunhofer, related to the spatial coordinates of the far-field on the screen. Expressed in the angle θ from the slit to screen and the k-vector amplitude $k_0 = \frac{2\pi}{\lambda}$

$$k_x = k_0 \sin\theta \tag{2.2}$$

The Fourier transform of the described aperture function with a top-head shape is a sinc-function. The visible intensity pattern would then be the square of this:

$$I_{out}(\theta) = I_0 \left(\frac{\sin(\frac{b}{2} k \sin\theta)}{\frac{b}{2} k \sin\theta} \right)^2 \tag{2.3}$$

Convolutions are useful tools in Fraunhofer optics because of their relation to Fourier transformations of multiplications of functions:

$$E_{out}(k) = \mathcal{F}\{t(x)E_{in}(x)\} = \mathcal{F}\{t(x)\} * \mathcal{F}\{E_{in}(x)\} \tag{2.4}$$

It is sometimes easier to calculate the Fourier transforms of the incoming field and the aperture separately, and then take the convolution.

2.2 Simple gratings with imperfections

Fraunhofer optics can be used to predict the transmission pattern of simple gratings. Comparing these calculations with experimental values of gratings made by the Nanoscribe should offer insight in what way imperfections arise. We can also include predicted imperfections into our grating model as an extra parameter.

The model for the grating will consist of rows long square bars of transparent material with a certain refractive index n. These bars have a height d, the distance through which the light will travel. They will be spaced apart the same distance as they are wide, which results in a periodicity a. The light is incident on the plane on which the bars are lined up and can either travel through the material of the bars or between the bars where there is a refractive index of 1. This will give rise to a phase difference ϕ between the different paths.

$$\phi = \frac{2\pi(n-1)d}{\lambda} \tag{2.5}$$

By choosing a convenient reference place halfway the height, we can write the aperture as a square wave of phase, as

$$t(x) = \begin{cases} e^{+i\phi/2} & \text{for every first half of a unit cell} \\ e^{-i\phi/2} & \text{for every second half of a unit cell} \end{cases} \quad (2.6)$$

which we could write down non-rigorously as:

$$t(x) = e^{\pm i\phi/2} = \cos(\phi/2) \pm i\sin(\phi/2) \quad (2.7)$$

With this, we can in principle use Fraunhofer and perform a Fourier transform.

$$E_{out}(k_x) = \int E_{in}(x) \cdot t(x) \cdot e^{ik_x x} dx \quad (2.8)$$

It would serve to leave out $E_{in}(x)$ from the first calculation because it is not intrinsic of the grating and we can take it into account later as by relation (2.4). What we are left with is the Fourier transform of $t(x)$. This has two parts: a constant of amplitude $\cos(\phi/2)$ and a square wave with amplitude $i\sin(\phi/2)$. The Fourier transform of the constant is a delta-function at $k = 0$ which represents the zeroth order. The intensity of the light in the zeroth order can then be found by squaring the amplitude:

$$I_0/I_{in} = \cos^2(\phi/2) \quad (2.9)$$

All the intensity other than the zeroth order should then be given by:

$$I_{rest}/I_{in} = 1 - \cos^2(\phi/2) = \sin^2(\phi/2) \quad (2.10)$$

How this intensity is divided over other directions can be found in the Fourier transform of the square wave part of $t(x)$. A square wave can be written as a Fourier series over all odd harmonics, positive and negative because the Fourier transform and diffraction pattern should be symmetric.

$$Squarewave(x) = \frac{2}{\pi} \sum_{-\infty,\,\text{odd}\, m}^{\infty} \frac{1}{m} \sin(\frac{m\pi x}{a}) \quad (2.11)$$

This can be interpreted physically as some discrete diffraction orders $k_m = \frac{m\pi}{a}$ with only odd orders. This is of course as expected from a grating. The intensity of every order is then given by:

$$I_m/I_{in} = \sin^2(\phi/2)\frac{4}{\pi^2} \cdot \frac{1}{m^2} \quad (2.12)$$

This result can be checked by comparing the sum of intensities of all the orders with the earlier conclusion from the intensity of the zeroth order alone in equation (2.10). The results are the same, as follows from the Basel problem, taking both positive and negative odd m.[13]

$$\sum_{\text{all odd m}} \frac{1}{m^2} = \frac{\pi^2}{4} \tag{2.13}$$

$$\Rightarrow \sum_m I_m / I_{in} = \sin^2(\phi/2) \tag{2.14}$$

From all this we can conclude some things on how the transmission pattern of the 3D-printed grating should behave like. First, there should only be odd diffraction orders in the far-field transmission. Secondly, the intensity of diffraction orders should decrease with order as $1/m^2$. Thirdly, the power of the zeroth order and higher orders are linked. How much light goes into either is determined by only the height d of the bars.

At the right height and wavelength combination all light can even be extinguished entirely from the zeroth order. This behaviour at the zeroth order can be interpreted by a simple light ray model. For the zeroth order, light comes straight out of the grating. The path of this light is either through the bar material, or the air between the bars. There is a phase difference between these paths. Because the areas of bar and air are the same, the amount of rays in each path is the same. If the phase difference is exactly half a phase, all rays through the bars are cancelled out by the equal amount of rays between the bars and no light is transmitted. The wavelength corresponding to the phase difference with no transmission can be measured in a spectrometer setup. From this the height of the grating can be determined.

If the light isn't entirely extinguished in the minimum, this could have multiple causes. One would be an unequal distribution of bar material and gap. If the amount of rays through the bars is unequal to those through the gaps, light will never be extinguished entirely, but the intensity also will never be maxed out to the zeroth order only.

A similar thing occurs when there is a variation of height in the grating. A bar could be a little higher than another, or the bar itself is not accurately written at constant height. This could be envisioned as the addition of multiple convex curves (I against λ) with different minimum wavelengths. At the minimum of one specific height, the curve of the others don't have a minimum and will lift the intensity to a non-zero value.

We investigate the effects of small displacements to the shape of one diffraction order by defining three ways of displacement of a grating bar. First there is variation in height of the bar. Secondly there is a variation in the thickness of the bar which varies the fraction of bar in one unit cell of period a. This is called variation of duty-cycle. Lastly there is variation in the position of the bar within the unit cell.

Any period of $t(x)$ of length a can be divided into t_{high} and t_{low}, where $t_{low} \equiv 1$ represents the part with no phase shift, while t_{high} is the bar part with acrylic material which causes the phase shift, with some small variation of that shift because of height differences.

$$t_{high} = e^{i(\phi+\delta\phi)} \approx e^{i\phi}(1 + i\delta\phi) \tag{2.15}$$

In a unit cell, t_{high} will be maintained for the first half from $x = 0$ to $x = a/2$. From there on, it is t_{low} until the end of the unit cell. However the beginning and end of any unit cell might vary. A variation in the beginning δx_a is interpreted as a variation in displacement. The variation of location of the end of a unit cell is given by δx_b. $\delta x_b - \delta x_a$ is the variation of duty-cycle.

Now to investigate the effects on an order by considering equation (2.8) around the diffraction order $k_1 = 2\pi/a$. $t(x)$ changes much faster than $E_{in}(x)$. So the idea is to calculate the integral for any period of $t(x)$ with $E_{in}(x)$ as constant. This will result in some function in x. The total $E_{out}(k_1 + \delta k)$ can then be calculated by taking (2.8) with $E_{in}(x)$ normally, but $t(x)$ is changed into that determined function, which is in principle the same for every unit cell with $\delta x_b$and δx_a depending on the unit cell.

$$\begin{aligned} &\int\limits_{\text{some unit cell}} t(x)e^{ik_1x}dx \\ &= e^{ik_1(x_{unitcell}+\delta x_a)}\left(\int\limits_0^{\frac{a}{2}+\delta x_a-\delta x_b} t_{high}e^{ik_1x}dx + \int\limits_{\frac{a}{2}+\delta x_a-\delta x_b}^{a} t_{low}e^{ik_1x}dx\right) \end{aligned} \tag{2.16}$$

$$\begin{aligned} \int\limits_0^{\frac{a}{2}+\delta x_a-\delta x_b} t_{high}e^{ik_1x}dx = t_{high}\left[\frac{e^{ik_1x}}{ik_1}\right]_0^{\frac{a}{2}+\delta x_a-\delta x_b} &= \frac{t_{high}}{ik_1}\left(-e^{ik_1(\delta x_b-\delta x_a)} - 1\right) \\ &\approx \frac{t_{high}}{ik_1}(-2 - ik_1(\delta x_b - \delta x_a)) \end{aligned} \tag{2.17}$$

and similarly for the second integral:

$$\int_{\frac{a}{2}+\delta x_a-\delta x_b}^{a} t_{low}e^{ik_1x}dx \approx \frac{t_{low}}{ik_1}(2+ik_1(\delta x_b-\delta x_a)) \tag{2.18}$$

Added together, integral (2.16) for any unit cell is:

$$e^{ik_1(x_{unitcell}+\delta x_a)} \cdot (t_{high}-t_{low}) \cdot \left(\frac{2i}{k_1}\right)(1+\frac{ik_1}{2}(\delta x_b-\delta x_a)) \tag{2.19}$$

This result can now be used for an integral over all x with $E_{in}(x)$ added in to determine $E_{out}(k_1+\delta k)$. The result from (2.19) needs to be normalised as per unit x and not per whole unit cell, which is done by dividing (2.19) by a.Also substitute t_{high} and t_{low} with their expressions in phase difference ϕ and $\delta\phi$. The end result is then:

$$E_{out}(k_1+\delta k) = \int \left(\frac{2i}{ak_1}\right) E_{in}(x)e^{i\delta kx} \cdot e^{ik_1\delta x_a}$$
$$\cdot \left[\left(e^{i\phi}-1\right)+\left(i\delta\phi \cdot e^{i\phi}\right)+\left(e^{i\phi}-1\right) \cdot ik_1(\delta x_b-\delta x_a))\right] dx \tag{2.20}$$

The calculation can be repeated for higher orders k_m, which yields the same result as formula (2.20) with substituted $k_1 = k_m$.

All variations cause a phase factor in the integral. Phase factors in the integral give rise to the need for deviations δk from k_1 to cancel them out. So variations cause a small covered range around k_1. This can be observed as an increase in width of the diffraction order.

The different variations have different impacts on the width. Height variations $\delta\phi$ effect all orders equally with a width increase because the associated phase factor does not depend on k_m. The effect from variations in displacement δx_a increases with higher order, which is also the case for variation in duty-cycle $(\delta x_b - \delta x_a)$. Both cause a width increase that is larger for higher orders. However, the effects from variation of displacement are stronger because the phase factor scales with $e^{ik_m\delta x_a}$, while the duty-cycle variance only scales with $ik_m(\delta x_b - \delta x_a)$. Typically, δx_a is also larger than $(\delta x_b - \delta x_a)$.

We can observe the optical effects of variations in the structure by measuring the width of diffraction orders. We expect a width increase compared to the perfect grating equal for all orders from height variations. We expect width increase that increases in magnitude with diffraction order from variations in displacement and duty-cycle.

2.3 3D printed flat en tilted planes

Simple structures that is worth investigating are flat surfaces. Especially for larger, more mesoscopic structures, parts may be flat. However, this can be problematic because of the discrete nature of 3D-printing. The technical details of discretisation are depicted in section 3.2. If suffices to say for now that large plane structures are 3D-printed continuously in one direction and discretely in the other, resulting in parallel writing lines. These lines are connected, but not square-like and so the lines emerge as a certain distance apart instead of a perfectly flat plane.

The same discretisation happens as well in the vertical direction. 3D structures consist of stacked planes, written a certain distance apart. Because these planes are integral to 3D-printing production, it is important to investigate the effect of 3D-printed flat surfaces on optics as opposed to for example mechanically polished surfaces. A flat plane will be made as a sample to investigate this. The expected transmission pattern for a perfect plane is just one dot, as if there was no sample. However, both the substrate and the sample flat plane would reflect part of the incoming light, resulting in the transmission dot having a lowered intensity. The 3D-printing production would result in specific cases of surface roughness, and the effects are discussed in section 3.2.

Furthermore, it is a goal to investigate the effects of the stacking of planes as a means of creating a solid with a shape. Investigating a plane with a gradient would showcase the problems that arise for trying to create rigid solids that would need smooth surfaces. A plane with a smooth gradient would refract the light on an angle, but with a 3D printer, the smooth gradient would have to be discretised in a staircase shape. This would have to act as a grating with the periodicity of the stairs steps.

A far-field diffraction pattern has been derived by the supervisor of this project. A 3D-printed tilted plane would have even and odd diffraction orders, the whole pattern shifted a refraction angle depending on the gradient. The intensities of the orders m fall off as:

$$I_m \sim \frac{1}{(m + \frac{\alpha}{2\pi})^2} \tag{2.21}$$

Where α is the phase difference between different stairs steps, with height steps L.

$$\alpha = \frac{2\pi}{\lambda} \cdot (n-1)L \tag{2.22}$$

2.4 Multi-layer structures

The end goal of this research is to produce periodic 3D structures. The way this will be explored is by stacking layers of gratings, with each layer rotated on an angle. Fraunhofer optics is useful to analyse the transmission of samples that have a clear aperture plane. This is not the case with any 3D structure. The 3D structure would have to be sliced in 2D planes, with the transmission wave of each layer being the incident wave of the next. However these layers would have little to no distance between them. You can not apply Fraunhofer by performing multiple Fourier transforms because the calculated fields only apply in the far field.

Another option would be to think of one aperture field that encapsulates effects of all layers and their interactions. However this mostly leads to gross approximations when multiple layers are involved.

However, Fraunhofer might still be used to try to understand what might happen in a sample with just two grating layers by ignoring light interactions that involve both grating layers and have both gratings act independently, which gives an aperture like this:

$$t_{tot} = t_1(x,y) \cdot t_2(x,y) \tag{2.23}$$

The second layer grating would act on every diffraction order of the first layer by splitting them into diffraction orders from the second layer. A lattice of diffraction orders would emerge on the far-field screen, with the two lattice vectors determined independently by the periodicity for vector length and the angle of the layers for vector direction. Because both gratings interact independently with the light, the intensities of the orders along lattice vectors should act like a single grating would, with a intensity fall off like $1/m^2$. If this is not the case, it can be concluded the gratings do not interact independently and this approximation does not work.

When the amount of layers increase to very large numbers, the structure can be better approximated by the properties of a photonic crystal. A photonic crystal has infinite periodicity in all directions. The optics in this crystal system can be calculated by applying Bloch's theorem to the Maxwell equations by assuming harmonic solutions with frequency ω and a k-vector, turning it in a eigenvalue problem.[3] The system is then characterised by the relation between ω and k, resulting in a band structure.

One interesting photonic crystal with a band gap, a range of ω without any states, is the woodpile structure. The woodpile consists of layers of gratings, every next layer turned 90°. Every second layer, which has parallel bars, is shifted sideways half a period as to fill the gap between bars of the parallel layer before it. This gives rise to a periodicity in the vertical direction of 4 layers.

A finite woodpile structure would not exhibit a perfect band gap. However, transmission of certain wavelengths should still be diminished, more so with more layers added.

Chapter 3

Method of production

The samples that will be researched here will have features that are smaller than a micron in size. Structures on this scale are conventionally produced with lithography methods. Lithography is a name for a collection of methods that in some way etch structure into a solid bulk material. Examples include etching with a solid needle, with an electron beam or a light beam on photosensitive materials.

While a lot can be made with lithography, not everything is possible. Cavities in the structure can not be produced and overhang is difficult in general, because the etcher has to approach from one side.
A solution for this is to build, instead of cutting away, and this is what a 3D-printer does. While 3D-printers have existed for a few decades, only recently have there been found methods to scale this idea down.

The machine that is used to 3D-print the samples in this research is the Nanoscribe, for a company of the same name. This is the chapter about how 3D-printing on a micro-scale can be done with this machine and the difficulties that this method of production causes in optical structures.

3.1 Two-photon polymerisation

The fundamental 3D-printing principle of the Nanoscribe machine is called two-photon polymerisation.
The basic setup consists of a basin with a solution of monomers and a laser-beam that is focused inside the solution. The laser light polymerises the monomers in the focus. The laser focus can move and in this way a polymer structure can be written within the solution. After the writing is finished, the solution can be washed away and the intended structure is

left.

This polymerisation process can be seen as a two-energy-state system for the monomers, with a low-energy unbound state and a high-energy polymerised state.
The photon energy of the laser can be chosen as exactly the energy gap, but another choice would be to use photons with half the gap energy. For the one-photon absorption, the light intensity that is absorbed would scale linearly with the intensity of the laser. However, for two-photon absorption, the absorbed intensity would proportional to the square of the laser intensity.
The laser intensity around the focus, which is the result of a Gaussian beam, is exponentially lower than the intensity right in the focus. Because of the different proportionality, the absorption intensity decreases faster around the focus for the two-photon than one-photon absorption. When the intensity is below a certain threshold, the polymer structure will not form a strong enough solid and will be washed away in the finishing process. The one-photon polymerisation also achieve smaller writing focus by using a smaller wavelength. However, the shape of the volume above the threshold is of a less useful shape (hourglass). The threshold edge is less well defined because of the slower decrease in intensity too, making the volume shape vulnerable to variations. Therefore two-photon polymerisation is the method of choice of the Nanoscribe.

You are limited in your materials for two-photon polymerisation. The monomers need to be sensitive to light (a photoresist material) and behave like the two-level system as described earlier. The samples that are made for this research are of an acrylic material, IP-Dip, which is transparent in the visible spectrum and has a refraction index of $n = 1.52$

3.2 Discretisation: Voxels and Writing lines

The size of the writing spot in the focus of the writing laser is of a finite volume. This 3D pixel, called a voxel, is the limiting resolution of the feature size of the structure. In the plane of propagation of the laser beam, x and y, the intensity around the focus decreases very rapidly as a Gaussian, while in the direction on propagation, z, it decreases more slowly. This results in a voxel that is longer in the z-direction than in the x, and y-direction. The shape of the voxel is similar to an ellipsoid.

The writing laser is moved with piëzoelectric motors, and is therefore discrete in movement. However, the step size can be much smaller than

the voxel size. A surface can thus be approximated by writing many voxels very close together, partly overlapping, as to approach a continuous plane. This is still an approximation and it would take infinitely many voxels to get this perfectly which would then take infinite time.
The best way to go about it for large structures is to have the writing laser turned on continuously and move it as continuously as possible as well. This results in a nearly continuous writing line. Lines can be written parallel to each other to fill a surface and there is then a choice for the density of these lines. This is the main source of discretisation.

The choice of the writing direction can be impactful on the faithful printed recreation of the digital design. A step function in height on a plane might be better written with lines parallel to the height step than with lines that all make the height step, because with the first option you place the discretisation right where there is one in the design.

The effect of these writing lines as a surface could be seen as some sort of grating with a very small period, just a few hundred nanometers. This is smaller than the wavelengths this research is concerned with. This means there will not be any diffraction orders, as the diffraction angle is larger than 90 degrees.

Another way to look at it is to interpret the writing lines as a surface roughness contributor that is probably of a higher amplitude than those caused by inaccuracies of the writing. Roughness causes random scattering as for example Rayleigh scattering.[12] However, this roughness from the discretisation is only in the direction perpendicular to the writing lines direction. It is then expected for scattering from writing lines that it is only, or mainly, in that perpendicular direction.

3.3 Accuracy

Even after the intended perfect structure is discretised into voxels, it is a question of accuracy whether the 3D-printer can actually make the structure as perfect as the software commands. Mechanical vibrations in the machine can displace the laser focus and thus the voxels.
It is hard to predict the quantitative sizes of these inaccuracies, as they vary per Nanoscribe machine and location. This Nanoscribe is located at the Fine Mechanics Department of the Leiden University.

Another possible effect on grating transmission pattern comes from a combination between the periodicity of writing lines and the variance in their location. With a long range period periodicity may emerge with a non-negligible height amplitude compared to the height of the main periodicity of the structure. This would be visible optically as extra visible orders, presumably with a small angles.

The variance in height caused by inaccuracy will mostly come into play as surface roughness. This would cause random scattering and loss of power in the transmission pattern that is wanted. Contrary to roughness from writing lines, this scattering should be independent of direction.

3.4 Laser power

The exact voxel size, both in width and height can be varied in the Nanoscribe by increasing the laser power. In standard conditions the height is minimally about one micron. This can be reduced further by decreasing the power further. However from that point the relation between power and voxel size is determined more by the environment of focus, which can be hard to determine and subsequently control. So in this experiment we limited ourselves with this one micron height.

It is also possible to use too much laser power. The liquid solution starts to boil when heated too much by the laser. Gas bubbles are not only a problem for the homogeneity as needed for optics, the fast expansion can cause mini explosions that destroy the surrounding structure and leave a small crater or cavity. These can contribute to random scattering of light.

3.5 Finding the substrate surface

The samples are printed on a substrate. In this case a very flat piece fused silica, $n = 1.46$ at $\lambda = 520$nm, that can be mounted in the experimental setups. The 3D-printer needs to start printing right at the surface to adhere. While the Nanoscribe is very good at making printing motions relative to earlier positions, finding the surface to start at can be difficult. Especially because it is transparent. When the writing laser is focused inside the solid substrate nothing really happens. There are no destructive effects on the substrate or something like that.

It is unavoidable to have some error in the starting height and it is better to secure fast footing than start printing above and disconnected from the substrate. This will result in some lower height compared to the digital design. As shown in section 2.2, for gratings the height is the deciding factor in the power distribution between the zeroth order and higher diffraction orders, but it might be hard to set this height because of this substrate surface problem.

The problem extents when the surface is not level with the x, y writing plane. A gradient of the substrate could result in a linearly changing height over the sample when the Nanoscribe does not write with the substrate gradient.

If the problem of surface finding turns out to be significant for our samples, a solution might be to print a flat plane underneath the actual structure to act as a height buffer. The height change will then only happen in the homogeneous material and in principle not effect the optics. This also gives another argument as to why the flat plane as a sample is interesting.

Writing inside the substrate can also be used to an advantage. While the voxels are one micron high, you can get lower structures by writing half of the voxel inside the substrate. This can not be done for any layers above the first one, but might still be useful.

3.6 Writing time

Another bottleneck in the production of samples is the writing time. While it might be technically possible to solve some of the problems, like discrete writing lines, it would take too much time to write it like that. When writing times might take more than 100 hours for one sample, you have to consider that there are more researchers using the same machine.

A 250x250 micron solid plane of one voxel layer with writing line distance 0.3 micron takes about 2 hours. Multi-layer gratings can take way longer, up to 100 hours for a certain sample with 9 layers in the case of this research.

The time per line increases when the writing laser on a line is not continuously turned on, meaning the lines have parts taken out. For example, writing a grating with the writing lines parallel to the grating bars would take shorter than writing perpendicular to the bars, because the latter would need to stop the laser between every bar.

In macroscopic 3D-printers it is custom to not fill up the solid parts of the structure, but instead use some rigid lattice. This saves a lot of time, but is not possible for structures with optical purposes as you need a homogeneous medium.

Chapter 4

Method of Characterisation

4.1 Transmission measurement setup

The optical properties of a grating can be investigated by illuminating it with a coherent light source, a laser. The light will be transmitted in a diffracted pattern. The optical properties of the sample can be characterised by looking at this transmission pattern and compare with what it should be from theory.

The setup that is needed to measure the transmission patterns from structures basically consists of a 520 nm CW laser that shines on the sample and a light detector behind it. However, there are there are more quantities that are necessary to be measured to fully characterise the transmission through the sample. A map of the optical transmission setup is found in figure 4.1.

The measured transmission light intensity is interesting as a relative value of the total in order to compare it to theory, so there will also be a measurement of the total laser beam power simultaneously with the transmission measurement. For this purpose, a flip mirror aimed at a photodiode detector is positioned between the laser and the sample. This makes it possible to toggle between detecting a transmission and the total laser power. This poses no problem on short time scales, as the structure, and thus the pattern is static. However on long time scales of more than a few minutes, the CW laser power might drift.

The diameter of the laser needs to be smaller than the sample size to only measure the optics of the sample, which will only be a 250x250 micron square. The laser will be focus the beam on the sample with a positive

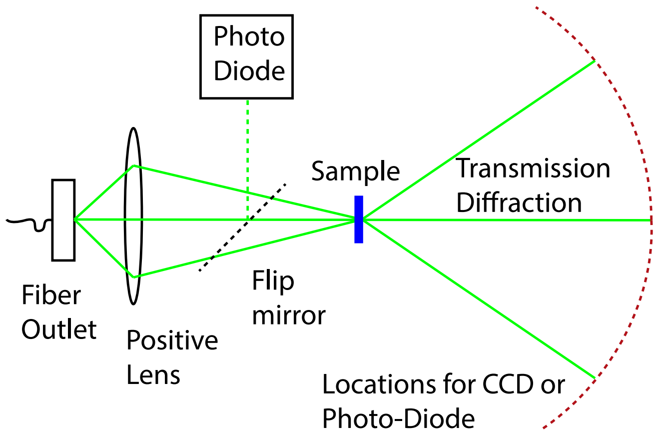

Figure 4.1: Schematic representation of transmission setup *The laser is connected to the fibre that enters the setup on the left. The light is weakly focused on the sample. Different detectors can be placed on the arc to investigate the angular dependant transmission pattern. The shape of the pattern can be imaged using a CCD camera, a photo-diode can be used to measure the intensity at different specific locations, or a white screen can be placed to investigate the pattern by eye. A flip mirror in front of the sample enables the measurement of the signal intensity incident on the sample with a photo-diode detector. The reflection on the substrate is inspected in order to position the sample inside the weak focus.*

lens. The light will not actually focus on a singularity, but focus weakly. For laser light focused by a lens, the light can be described as a Gaussian beam. This means that at the weak focus, right between the transition from converging to diverging light, the light will have a Gaussian intensity distribution in the plane of propagation, and the same phase in that plane.

In this setup, the laser light will come from a glass fibre. The finite diameter of the outlet results in a divergent beam. So the role of the lens right behind the fibre is both to straighten the divergence and create a weak focus of the sample.

To determine the quality of the beam, and how good it follows the theory, you can relate the width in the focus, w_0, with how it changes out of focus in the direction of propagation, $w(z)$. According to the theory of Gaussian beams, w changes hyperbolic with z:

$$w(z)^2 = w_0^2 \left(1 + \frac{z^2}{z_0^2}\right) \text{ with } z_0 = \frac{\pi w_0^2}{\lambda} \tag{4.1}$$

In a simple experiment with a beam profiler, the Gaussian width of the beam in this setup was determined for different z by fitting Gaussians over the profiles. A hyperbolic fit was performed over these measured $w(z)$ and the w_0 and z_0 of our setup were found for both the x and y direction.
The quality of the beam is determined by the quotient[14].

$$M^2 = \frac{\pi w_0^2}{\lambda z_0} \tag{4.2}$$

Which according to relation 4.1 should be 1 if the beam is perfectly Gaussian. The properties of the beam in our transmission setup can be found in table 4.1.

Direction	w_0 (in μm)	z_0 (in mm)	M^2
x	68.2 ± 1.8	25.3 ± 0.8	1.11 ± 0.06
y	68.4 ± 1.6	25.6 ± 0.6	1.10 ± 0.05

Table 4.1: *Table with properties of the focused beam in the transmission setup, which is supposed to be Gaussian. For this to be the case, M, which is determined by relation 4.1, should be equal to 1. The values for M_x^2 and M_y^2 are good enough for this experiment. Another important property is the beam width w_0. This is defined by the width where the Gaussian intensity profile in the focus of the beam has decreased with a factor e^2 from the peak. The samples that are illuminated are 250x250 micron in size, meaning when the sample is in the centre twice this width should stay under 250 micron. Lastly, z_0 is a measure of how quickly the beam widens around focus. This is again depicted in relation 4.1. A larger value of z_0 corresponds to a slower widening. This is useful in this setup, as samples might have a finite thickness. With a sharp focus it might be hard to have all of the sample in the focus. Also, it is easier to mound the sample sufficiently in the area with small enough width with a weak focus.*

It is not a trivial task to locate the small sample on a large substrate at the weak focus. An extra camera was used for inspection of the sample. A lens will image the reflection of light on the substrate, and this was used to position the sample in the weak focus.

In the far-field behind the sample a CCD can be placed, aimed at any angle. The shape of a diffraction order can be captured with the CCD.

From theory section 2.1, we know the transmission pattern is given by the convolution of the Fourier transformations of the aperture and the incident field and from section 2.2 we know Fourier transformation of the aperture for a grating should consist of δ-functions ideally. In this setup, the incident field is of Gaussian shape, for which the Fourier transform is itself a Gaussian. With this, we expect the diffraction orders to mimic this Gaussian shape in the transmission far-field. Another conclusion from section 2.2 is that displacement and variation in duty-cycle of the grating result in a spread in the angle of a diffraction order. In this setup, a spread in angle would mean a wider Gaussian shape of the diffraction order. Imperfections would then be noticed optically as increasing width of diffraction orders with higher orders.

Actually, there is a natural increase in width in perfect gratings stemming from the fact that the above conclusions where given in k_x, which is angle dependant as in identity (2.2), while the width is measured in terms of a range of angles on the screen.

$$\Delta k_x = k_0 \cos(\theta) \Delta\theta \tag{4.3}$$

This results in a natural increase of width with a factor $1/\cos\theta$ The effect of grating imperfections is to widening the Gaussian shape of diffraction orders on top of the natural increase in width.

An important property of gratings for practical purposes is how the transmitted power is distributed over the diffraction orders. As shown in section 2.2, the power should decrease inverse quadratically with diffraction order. For titled planes, we expect a difference in power between positive and negative orders and, as shown in section 2.3, these differences can say something about the discretisation of the gradient. The power of a diffraction order can be measured with a photo-diode intensity sensor instead of the CCD camera. To be able to compensate for a slightly fluctuating laser intensity, the incident intensity on the sample is also gauged with a second photo-diode in the path of a flip mirror.

4.2 Spectrometry

Spectrometry can be used to investigate the effects of the height of gratings on the optics, as depicted in section 2.2. A transmission spectrometry setup made by Michiel de Dood and Daniële van Klink is used. This experimental setup uses a halogen light with a continuous spectrum. This light is emitted into a fibre. The fibre light is focused on the sample in a similar way as in the laser transmission setup. The transmitted light is coupled into a fibre which leads to a spectrometer. The sample mount is rotatable with the rotation axis at the sample's centre. The spectrometer fibre is located on an arm which can turn with the sample as point of rotation.

For the gratings, only the zeroth order is analysed with incident light straight at the sample. However this setup enables the measurement of the band structure of samples by varying the incident k of the light by changing the angle of incident with the rotation of the sample. This can be used to analyse woodpile samples.

4.3 AFM

It is also useful to see what structure is actually printed to confirm the relations between structure and optics. While optical microscopes are an option and definitely useful to get a overview of the 250x250 μm structures, the structures that are printed have features that are smaller than the visible wavelengths, like writing lines. These features are of interest and are impossible to image with a microscope as they are under the diffraction limit. Another shortcoming of optical imaging is the difficulty of imaging the height.

Various other micro-imaging techniques are available, however any electron microscopy technique is problematic because the sample's material is an insulator. We have special interest in height measurements and so the chosen micro-imaging option is Atomic Force Microscopy (AFM). This technique images with a solid needle driven to a frequency. If this oscillating tip approaches matter, it is influenced by the atomic electromagnetic force of the matter. From the effect of these forces on the driven oscillation, the structure of this matter can be mapped.

The tip approaches from one direction and maps the height at each point. Depending on the complexity of the structure, the height can be determined up to less than ten nanometers. The height is therefore a fine metric describing the general structure of gratings with alternating high and low areas with height difference of a few hundreds of nanometers. Additionally, AFM is also sufficiently accurate to image the surface roughness and writing line features.

Another goal of using AFM is to investigate whether the Nanoscribe's problem in finding the substrate surface does actually cause problems as suggested in section 3.5. Expected effects concern an overall gradient in the height. The AFM available at the Leiden University can only image areas of 30x30 μm at the time. Any gradients that are smaller than what can be measured in that interval might be hard to determine.

Chapter 5

Results on simple gratings

Three different gratings have been 3D-printed for this research project. All three are designed to have a square wave shape with a duty-cycle that fills half the period as to have the bars width equal to the space between the bars. The three gratings that are researched differ in their periodicity. The gratings have a periodicity of 4 μm, 2 μm, and 1 μm. The height of the bars for all three gratings is designed to be 1 μm. In an effort to avoid the problems of substrate surface finding encountered in the first grating, the two finer gratings have been printed on top of a 3D-printed flat plane that acts as a buffer layer.

The samples cover a surface of 250x250 μm in a square shape. Optical microscope images of the samples can be found in figure 5.1 The bars are written straight and parallel. However, from these images small displacements can be seen which would influence the optical transmission pattern as derived in section 2.2.

Figure 5.1d shows one of the early 3D-print samples of the 4 μm grating that failed. One of the Nanoscribe settings that was off and needed adjusting was the writing laser power. The power was too high and gas bubbles were created. Surprisingly this only occurred on one side of the sample. This was a clue that there was a gradient in the sample, possibly caused by the difficulties of the Nanoscribe to find the substrate surface. The 4 μm grating was printed in the same 3D-printing session and on the same substrate. It was suspected the gradient would be present for all the samples, even if a lower laser power prevented gas bubbles. Consequently, measures were taken to prevent problems with surface finding, like the introduction of a flat plane as buffer layer.

The reason why a gradient was suspected, was because a gradient causes partial loss of effective power in the writing laser focus. For the parts without bubbles most of the laser power in the focus would be inside the substrate where it could not evaporate any liquid, however for the parts with bubbles most of the laser focus would be located inside the solution and would have enough power to heat the liquid into evaporation.

In the optical images of the gratings you can see some samples darker than others. Darker samples could have more light scattering. It is surprising that the samples with gas bubbles seems to scatter less light than the sample without the bubbles that is used in the end. This suggests there is a more ideal writing laser power that does not create gas bubbles, but does produce better internal or external structure.

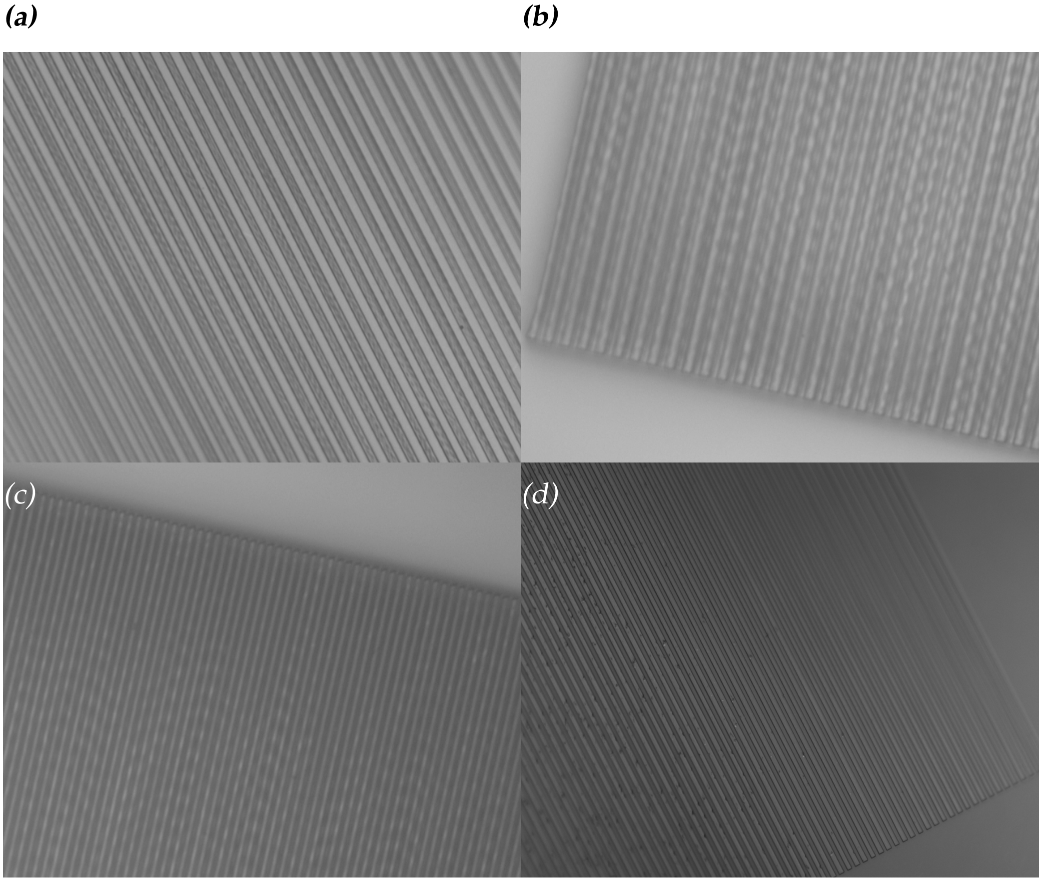

Figure 5.1: Optical Microscope images of 3D-printed gratings.
(a) shows the 4 μm grating. The bars are slightly squiggly, displaying unintentional displacement in this grating. Periodic features are visible on the surface of the bars, hinting to a rough surface. The 2 μm grating is shown in (b). This one is printed on a flat plane as layer between grating and substrate, so the substrate is not visible between the bars. The bars seem even more squiggly, but this could be a artefact. (c) is the even finer 1 μm grating. The grating has a higher duty-cycle that the intended 50%, especially at the bars in the top left . (d) shows a failed version of the 4 μm grating. Too high writing laser power led to evaporation explosions, which can be seen here as black spots in broken bar parts. Curiously, they only occur at one half of the sample. A possible explanation for this would be a height gradient in all of the sample, resulting in less power on one half by having the laser focus aimed partly inside the substrate there.

5.1 Transmission

As can be seen in figure 5.2, there where more orders visible than just the predicted odd orders. For the 4 μm grating, there were unexpected orders which turned out to have 1/3 of the main diffraction order angle. This suggested an extra periodicity of three times the length of the main periodicity. Looking back closely at the software structure input for the Nanoscribe, it turned out the software responsible for automatically discretising the perfect design made a rounding error and shortened every third bar with one writing line. This problem has been avoided for any consecutive grating structure.

An unexpected feature of the gratings that was consistent across all grating versions was the existence of the even orders. The second orders are weak, about a factor 1000 compared to the first order. The shape of the order is not Gaussian, but rather a stain. It follows from theory that they should not exist. The source of these even orders is probably the imperfection of the grating, but it is unclear what aspect of the imperfections have resulted in the even orders.

Weak diffraction blobs are distributed randomly on the line connecting the diffraction order in all gratings. They are more intense in proximity to the main diffraction orders. This feature will from now on be called the blob line. The blob-like nature of the line suggests that the source has some sort of periodicity, opposed to the line being continuous. The scattering line occurs only in one direction. The vertical line in the pattern leaving from orders in figure 5.2 is of a different nature and is simply a sinc-like diffraction pattern emerging from the finite square shape of the sample. This will be discussed further in section 7.1.

The alignment of the blob line with the grating orders suggest the source has periodicity in the same direction as the grating, and the small angle suggests that this period is large compared with the grating. A good candidate for the cause are the writing lines, that fit the alignment criteria. Displacement of writing lines might create random long range periodicity.

The intensities of the diffraction orders can be seen figure 5.3. For the largest 4 μm grating, the inverse squared model holds fairly well, while for the finer 2 μm grating the intensity falls off faster than theory which suggests there is more power loss in this grating. The finest 1 μm grating only had one visible diffraction order on both sides, so no trends could be found.

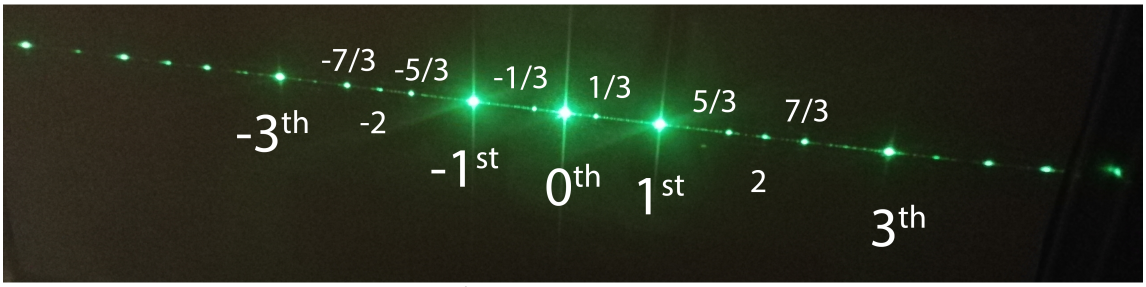

Figure 5.2: Transmission pattern of 4 μm gratings.
The pattern was projected on a screen and photographed. This was the first sample created. While only the odd orders were expected, many others showed up. The source of the even orders are probably imperfections of some sort. There are orders visible that have diffraction angles a third the size of the main orders. The origin of these should be a periodicity of three times main periodicity. It was later found that a software rounding error shortened every third grating bar with one writing line. This problem has been prevented for all other samples. There is a horizontal line and there are vertical lines crossing at every order (the diagonal line is an artefact of the mobile camera used) . The vertical lines seem evenly illuminated, but the horizontal line connecting all orders consists of many blobs of light, acting as a band of randomly placed and weak diffraction orders. This blob line also appears in the other grating samples

The widths of diffraction orders can be found in figure 5.4. Both the 4 and 2 μm grating show displacement and/or variation in duty-cycle, the latter more than the former. The horizontal width is also higher than the expected lowest width for a perfect grating, which can be determined from what the Gaussian beam would do without any sample. This shows there is also height variation.

***(a)** 4 μm grating*

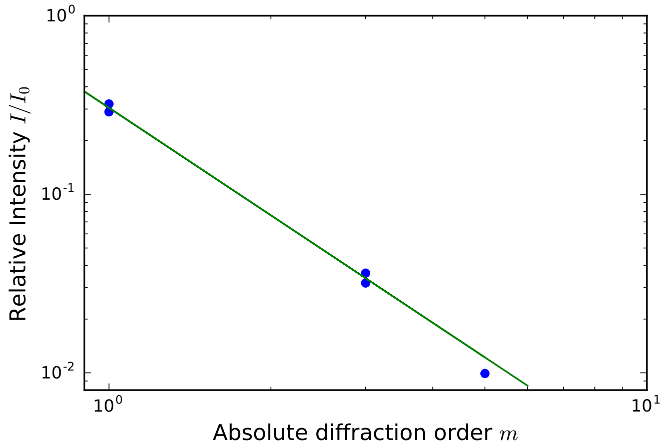

***(b)** 2 μm grating*

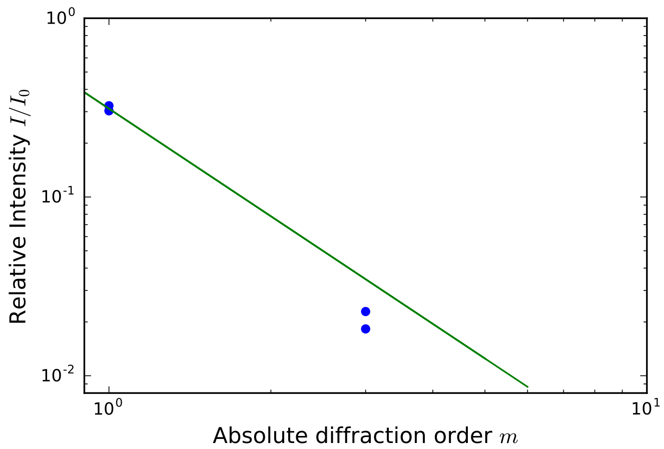

Figure 5.3: LogLog-plot of intensities of diffraction orders in the transmission pattern of gratings.
Both positive and negative diffraction orders are shown with their absolute value. Even though the orders should be symmetric in power, a slight wedge in the sample position or a height gradient could divide the intensity unequally. The green line is an inverse square fit, with a gradient of -2 in a loglog-plot. (a) shows the 4 μm grating data. A data point for the positive 5th order is missing, because the path was blocked for the CCD. However, looking at the trend from lower order data points, it could be hypothesised the +5th order would average out the deviation from the -5th order. With this, the 4 μm grating would follow theory well. The 2 μm grating in (b) shows clear deviation from theory, with a faster decay in intensity in higher orders. This light is scattered away in other directions.

(a) *4 μm grating*

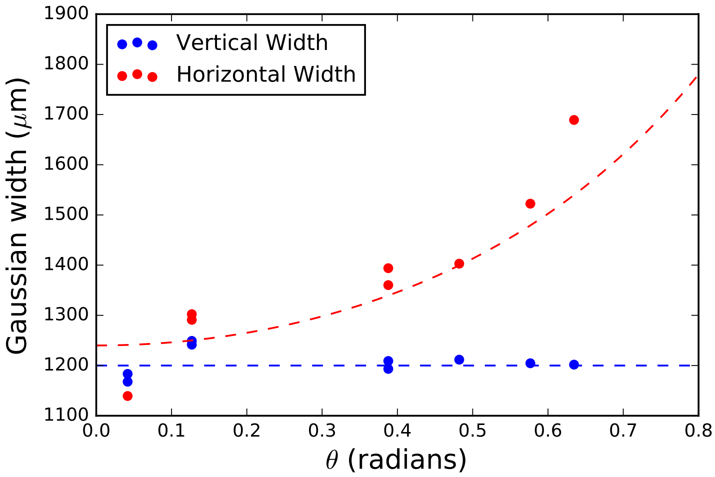

(b) *2 μm grating*

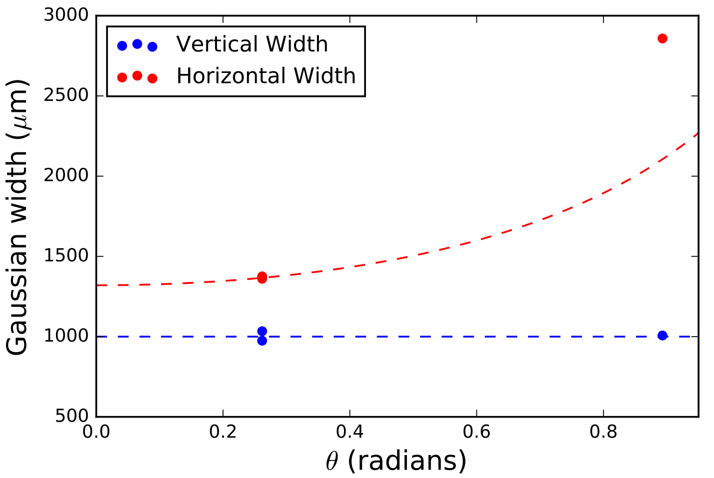

Figure 5.4: Gaussian width of grating diffraction orders.
Plotted are both the horizontal and vertical widths of the Gaussian shaped orders. The width was measured at 390 mm from the sample. The angle in the vertical direction is zero for every order, which are diffracted in the horizontal direction only. Therefore the vertical width should not change with order. This constant width is plotted in the dotted blue line. In the horizontal direction the angle does change, which results in a natural growth in width with a factor $1/\cos\theta$*. This is plotted with the dotted red line. Any more growth must come from displacement and variation in duty-cycle. Both the 4 μm grating in (a) and the 2 μm grating in (b) show a larger growth than the natural growth, which we attribute to variations in displacement and/or duty-cycle.*

5.2 Spectrometry

The specta of the zeroth order of the gratings can be seen in figure 5.5. The 4 μm grating shows a minimum transmission of 0.4, which indicates a large range of heights in the sample. We expect this to be a height gradient originating from the surface finding problem, because the other samples have had extra measures to prevent this and do have a minimum close to zero. While the fits seems to show the theoretical model is correct, they indicate a sample height which is less then half the intended height. These heights could be physical, or merely effective heights.

(a) 4 μm grating

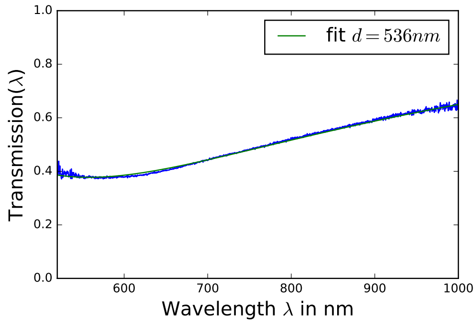

(b) 2 μm grating

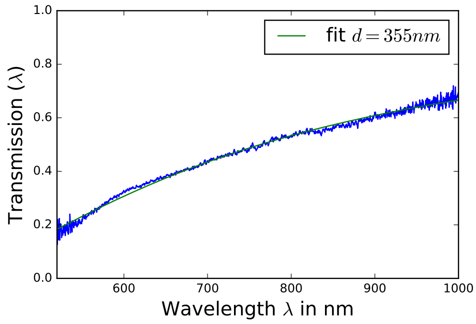

(c) 1 μm grating

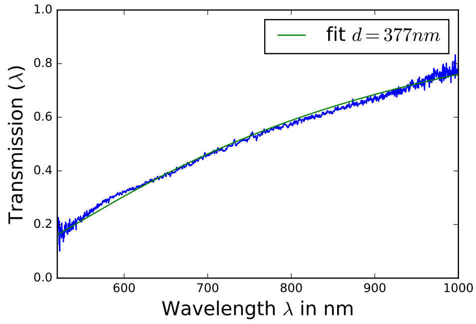

Figure 5.5: Transmission spectrum of zeroth diffraction order of gratings. *The blue line is the measured transmissions at different wave lengths, corrected with a dark measurement and normalised with a light measurement. The green line is a fit of the zeroth order intensity as given by formula 2.9, dependant on the height d, with an amplitude factor before the squared cosine to account for reflected, scattered and absorbed light. (a) is the 0th order spectrum of the 4 μm grating. Because the minimum is not located at (almost) no transmission, an offset fit parameter was added. This parameter represents effects from height variation. The 2 and 1 μm grating, respectively in graph (b) and (c), were fit without the need of an offset and conform to theory. The theory does not account for the slight hick up around 600 nm present in both (b) and (c). The grating heights gotten from this spectrum are 536, 355 and 377 nm for (a), (b), (c) respectively. This is lower than half of the intended height for the other sample. This low height and need for an offset parameter suggests the μm grating has a height gradient, because imperfection variations don't have this scale. This means the found height for (a) is more of an effective height. The 2 and 1 μm samples have the same height, which is still well defined shown by a minimum close to zero. This suggests yet a different cause of low height than for 4 μm.*

5.3 AFM

The AFM images of the three gratings can be seen in figure 5.6, together with height profiles taken from these images. The AFM image of the 4 μm grating shows up as having the intended flat shape at the top, with visible writing lines. The edges of the bars do not go down straight, but on an angle of 45°in this AFM image. The shape deters from the intended rectangular shape with even lower angles for the gratings with smaller periodicity. The geometry of the cantilever tip forms a fundamental limitation to any AFM measurement. The used cantilever tip was 500 nm high sharpened tetrahedral with the hypotenuse on a 35°angle, ending on a point of diameter 7 nm. Most likely, the width of the cantilever limited the reachable depth between bars, creating an apparent V-shaped gap in samples with smaller periodicity. This would leave the AFM images as unreliable around the bar edges, and for the finer samples in the entire gap. Alternatively, the voxel width was larger than expected and filled the gap by connecting prematurely. However, the spectrometry measurements do not support this view. Those give a height about 200 nm higher than the 150 nm in the in the AFM image. The intensity in the diffraction orders in transmission also have higher intensity than would be expected for heights given by the AFM. The existence of the even diffraction orders does support the view that the AFM image is correct. These orders that should not exist in a grating with rectangular shaped bars, but the AFM images show this rectangular shape might not be there, which would give rise to the even orders.

Either way, the right periodicity is maintained also for the finer gratings, but duty-cycle is way higher than the intended half of the periodicity. There is also displacement of the whole bar for all samples. This would then confirm the origins of the increasing widening of the diffraction orders in transmission. Assuming the AFM image is correct, the cause of the increased duty-cycle looks to be the edges of the grating bars that don't end vertically, but fall off slowly and widen the effective grating bar.

It was motivated to look for a gradient in the sample caused by Nanoscribe surface finding problems as described in section 3.5 as a reason for reduced height. By making more AFM pictures at different places on the sample, the gradient was confirmed to exist in the 4 μm sample. This underscores the relevance of surface finding. The height in this sample ranges between 0.8 and 0.4 μm gradually perpendicularly to the direction of the bars over the 250 μm length of the sample. This explains the offset in the fit needed to describe the zeroth order spectrometry measurements of this particular sample. The found spectrometry height can then be seen as some effective height. The large height gradient would also explain the halfway divided areas with and without gas bubble mistakes in the failed sample. There is less power to evaporate the monomer solution if the writing laser focus is partly inside the substrate.

The writing lines are clearly visible on the structure. The amount of lines per bar is consistent with the instructions given to the Nanoscribe. This gives rise to a periodicity of writing lines of about 150 nm. This is indeed lower than the wavelength in the transmission setup and so the direct periodicity would not result in extra diffraction orders. From the AFM image of the 4 μm grating the missing writing line every third bar is clearly visible. This confirms the software discretisation mistake that was made in transforming the ideal grating model into the writing order to the Nanoscribe and explains the one-third orders.

The explanation for the blob line originating from long-range periodicity by displacement of writing lines stays plausible as there are variations in displacement visible of the individual writing lines on the grating bars. The height of the writing lines is around 10 to 20 nm for the finer gratings, but 100 nm for the larger grating. This is small compared to the other relevant characteristic lengths of the structure. The height of the bars is about a factor 10 larger than the variation in height from the writing lines. This does diminish the relevance of possible long-range periodicity, because effects from the writing lines would have a way smaller amplitude. Auto-correlations of the AFM height profiles (not shown) show no sign of long range periodicity for the limited area that can be probed by the used AFM.

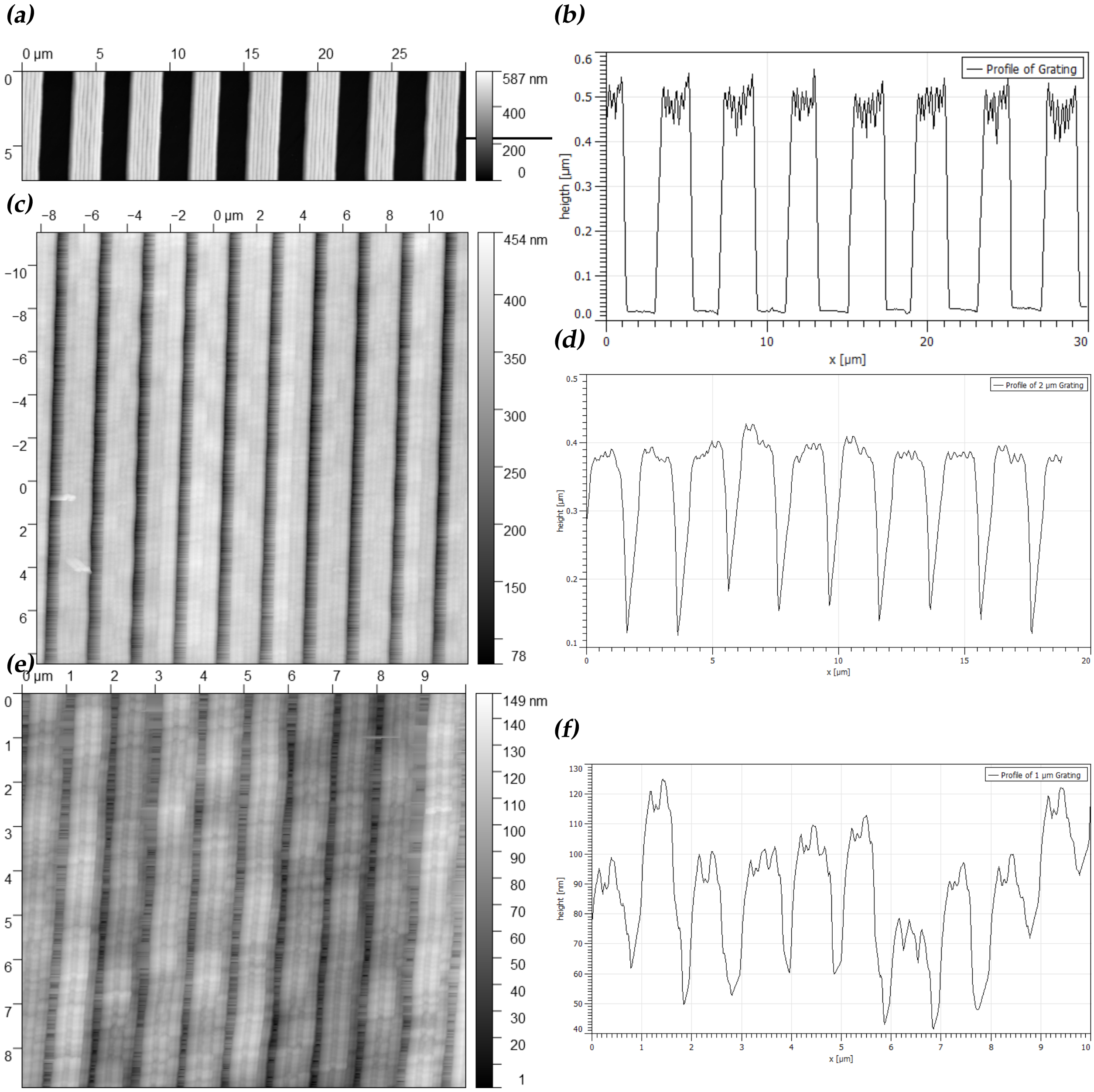

Figure 5.6: AFM images of 3D-printed gratings and profiles taken perpendicular to the grating bars.
The writing lines are visible in all gratings. (a) and (b) show the 4 μm grating. looks more square than the others, mostly because the gaps reach the flat substrate bottom. The missing writing line every third bar is visible. (c) and (d) show the 2 μm grating. The height is shortened and the gap is V-shaped, not reaching the bottom. The 1 μm grating, shown in (e) and (f) has that same gap feature and has even more rounded bars. Visible here, but true for all gratings, is that the height variation is about the same parallel and perpendicular with the bars, however the writing lines offer regularity in the latter.

Chapter 6

Results on flat & tilted planes

Three samples were produced to investigate of the optical transmission of 3D-printed flat surfaces. The first sample was simply a 250x250 μm flat plane with a height of 1 μm. A optical microscope image can be seen in figure 6.1 Some structure apart from total flatness can be observed in this image.

The other two samples are both samples of the same size, but with a slow gradient from a height of 2 μm to zero. However, the software of the nanoscribe decides that the tilted surface is not written smoothly, but is instead written by stacking thin layer planes, each a little shorter on one side as to form a discrete stairs structure. The stairs decent of 2 μm is done in 7 steps with constant height and periodicity.

Two versions of the tilted plane were written. One has writing lines parallel with the gradient, while the other has writing lines perpendicular on the gradient. In the optical microscope images the distinction is clearly visible. The tilted plane with parallel writing lines is darker and individual writing lines are visible as squiggles. These messy writing lines could lead to more power loss from diffraction orders to random scattering. The perpendicular written tilted plane sample is more similar to the flat plane sample on the flat parts, and with that more transparent.

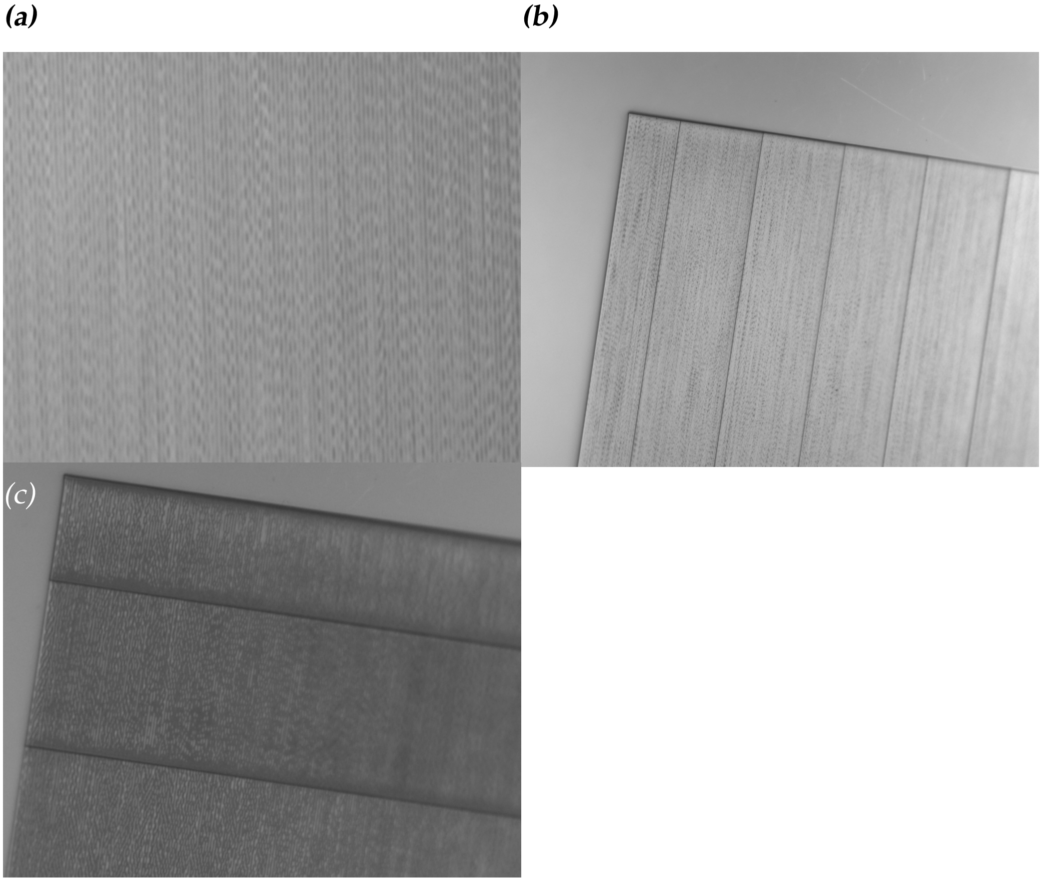

Figure 6.1: Optical microscope images of 3D-printed flat plane and tilted planes.
(a) shows the flat plane. One expects to see no features at all, but there are thin lines in vertical direction, accompanied by a light-dark pattern semi-periodic in the vertical direction. These could be due to height variations. (b) displays a tilted plane, written perpendicular to the gradient. The stairs-like planes that form the gradient are clearly visible and periodic. The edge is well-defined. The flat surfaces on this sample are similar as on the flat plane. This is not the case for the tilted plane in (c). There, the writing lines are visible as black squiggles. The overall structure is the same, with well-defined edges between layers. The black colour suggests a lot of random scattering or absorption. The first is more likely, because the sample material is transparent.

6.1 Transmission

The far-field transmission pattern of the flat plane can be seen in figure 6.2a. There only a zeroth order, however the blob line, with irregularly located light blobs on a line as also found in the grating transmission, and the vertical square sample diffraction are still there. The only features of the flat plane are the writing lines, so this means the origin of the blob line can not come from the bar shapes. The orientation of writing lines in figure 6.2a is vertical. This suggests the writing lines produce a blob line perpendicular to their orientation.

The far-field transmission pattern of the tilted planes can be seen in figure 6.2b and c and show diffraction order patterns, as hypothesised. Even and odd orders are visible. The small order angles correspond to the writing plane spacing of the samples. Except for the normal diffraction orders including the zeroth order, there is another zeroth order visible which represents the non-refracted zeroth order. The rest of the diffraction grating order pattern is shifted with an angle dictated by the refraction angle of the tilted surface. The origin of this straight ahead beam is most likely the light leaking around the square sample.

While the perpendicular written tilted plane does show the blob line, again between the diffraction orders, there does not seem to be a sign of the blob line in the parallel written sample. The light between orders for this sample is not characteristically blob-like. If the writing lines were responsible for the blob line, a vertical blob line might have been expected for this sample. However, it can also be the case that the sample is of not good enough quality. The parallel written tilted plane is the only one layer sample made where the periodicity from the grating does not line up with the periodicity in writing lines.

The intensities of the orders are graphed in figure 6.3 and correspond to theory well for sample with perpendicularly written lines. Conversely the order intensities for the parallel written sample are messy. This substantiates the argument that this sample has many imperfections.

The orders width can be found in figure 6.4. The horizontal widths are all larger than 1040 μm, the undisturbed Gaussian beam width on the screen at this distance, showing height variations. However, no further conclusions could be made about the displacement by comparing the growth of widths with the natural growth because for both samples the widths varied too much in the horizontal direction.

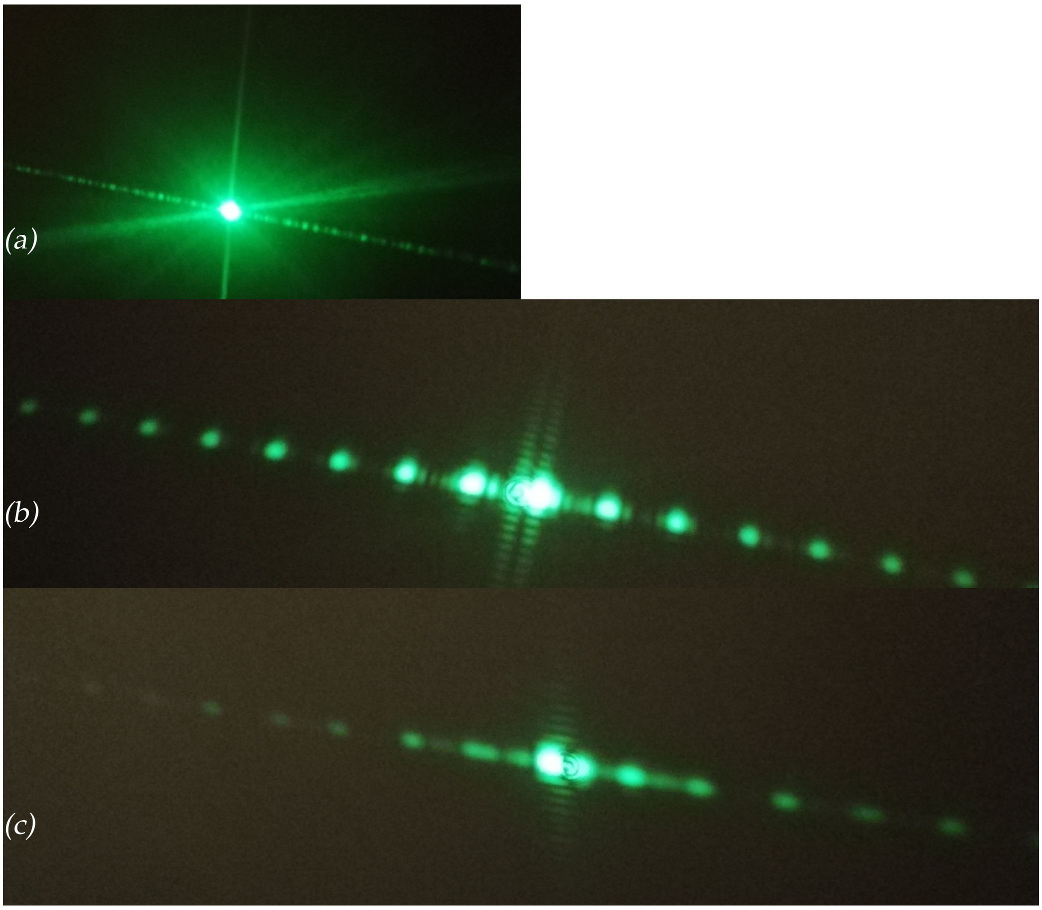

Figure 6.2: Transmission pattern of flat and tilted planes.
(a) shows the only transmission beam of the flat sample. The spot is very bright, with a transmission of 0.96. However, the vertical line and the horizontal blob line are also present here, proving that they are not grating related. (b) is the transmission pattern of the perpendicular written tilted plane. For this picture, the screen was moved from it's usual distance of 39cm to about a meter to be able to capture the patterns. The diffraction order pattern is there, but there are two zeroth orders. One is placed at the right angle to fit the zeroth order role in the overall diffraction pattern, but the other one is the undisturbed beam that is not refracted by the tilted plane. Both zeroth orders have vertical lines, which are actually diffraction patterns with lines. The origin of this pattern is the square aperture shape of the whole sample. The blob line is also there between the orders. (c) is the parallel written plane. This transmission pattern is more messy, as expected from the optical images. There is still something between the orders, however it is not blob-like as the blob line. In this sample, the periodicity of the writing lines is not parallel with the main periodicity of the sample. This is another hint at the connection between writing lines and the the blob lines.

(a) *Perpendicular-written tilted plane* ***(b)*** *Parallel-written tilted plane*

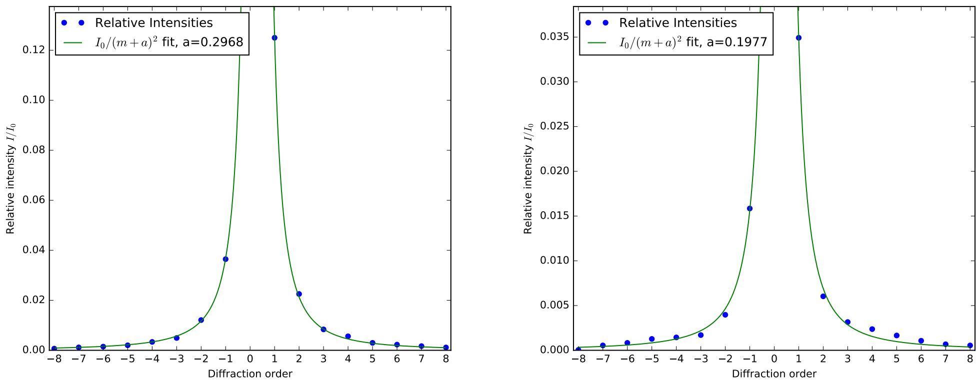

Figure 6.3: Intensities of diffraction orders in tilted plane transmission pattern. *The measured intensities of diffraction orders are the blue dots. The green line is a fit from the theory in section 2.3, which dictates* $1/(m+a)^2$ *with* m *the order and* $a = (n-1)L/\lambda$ *the optical path difference as in definition (2.22), with* L *the stairs step height. As shown in (a), the fit works well for the perpendicular-written tilted plane. However, the fit fails for higher orders for the parallel-written tilted plane, displayed in (b). The experimentally found* L *are 0.297 and 0.197* μ*m respectively, which can be compared to the intended value of* $L = 0.286\mu m$*. The parallel sample shows a large deviation here as well, underlining the the inferiority of the parallel-writing. The overall transmission intensity is lower in (b), too.*

***(a)** Perpendicular-written tilted plane*

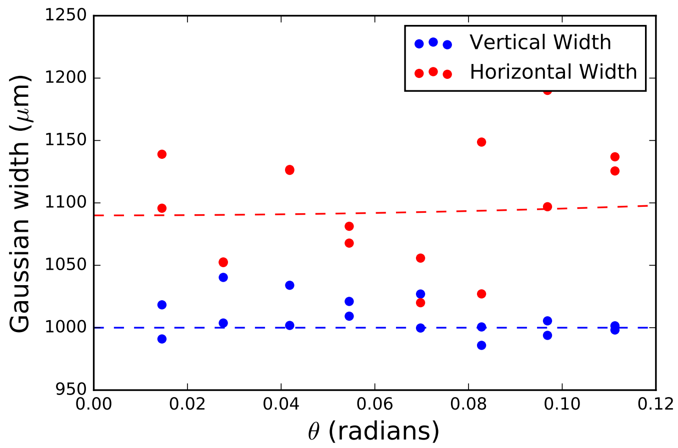

***(b)** Parallel-written tilted plane*

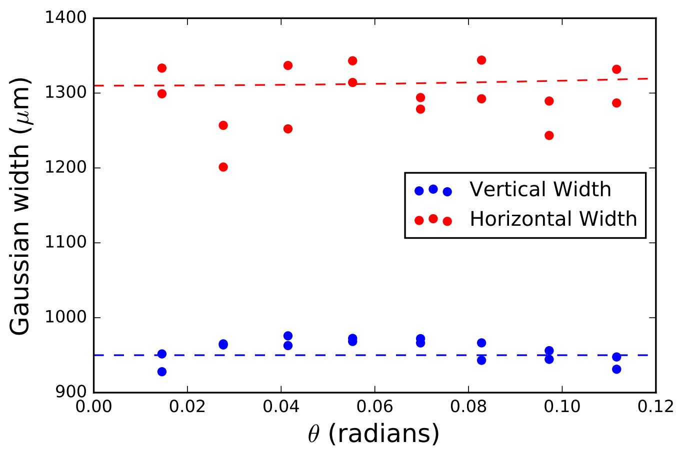

Figure 6.4: Gaussian width of tilted plane diffraction orders.
Similar as with the gratings in figure 5.4, both the horizontal and vertical widths of the Gaussian shaped orders are plotted. The width was measured at 390 mm from the sample. The angle in the vertical direction is zero for every order, which are diffracted in the horizontal direction only. Therefore the vertical width should not change with order. This constant width is plotted in the dotted blue line. In the horizontal direction the angle does change, which results in a natural growth in width with a factor $1/\cos\theta$*. This is plotted with the dotted red line. Any more growth must come from displacement and variation in duty-cycle. For both the perpendicular-written tilted plane in (a) and the parallel-written tilted plane in (b) is it inconclusive whether or not the structure has displacement. The widths do vary a lot, also in the vertical direction.*

6.2 AFM

We made an AFM image of the flat plane, which is shown in figure 6.5, together with profiles taken parallel and perpendicular to the writing lines. Just as with the grating AFM images, the writing lines are definitely present in the sample. The periodicity is equally short. Interestingly, the variation in height is actually similar for parallel and perpendicular direction, but it is only coherent in the perpendicular direction. This could explain the difference in scattering from horizontal and vertical direction.

In this AFM image it is visible that there is not only height variation on the short length scales of the writing lines. There seems to be some variation in height of the flat plane on a length scale of 3 or 4 μm. This length scale was confirmed with an auto-correlation (not shown). This is the basis on which to propose another theory for the origin of the blob line. The long distance periodicity could not come from displaced writing lines, but could instead be a structural periodicity in height caused by a mechanical vibration during the 3D-printing process in the Nanoscribe.

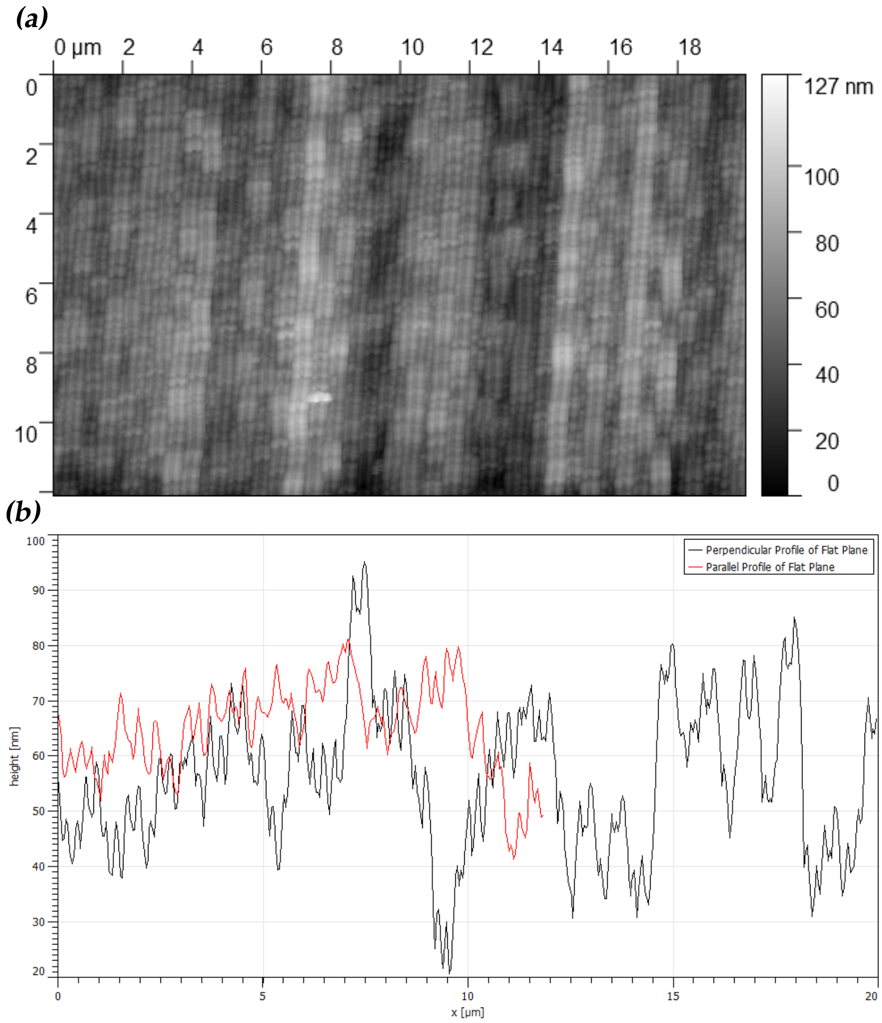

Figure 6.5: AFM image of a 3D-printed flat plane with profiles parallel and perpendicular to writing lines.
(a) The AFM image shows the semi-periodic black and white pattern in the vertical direction from the optical images in figure 6.1 as height variations on a length scale of 2 micron. The vertical lines that were visible in the same figure seem be to caused other height variations in the horizontal direction. These have a length scale of 4 micron and the edges are more sudden steps. The cause of these during printing is unknown, but it can be the reason for the long range periodicity causing the blob line. These observations about the flat plane surface are highlighted in the profiles in (b. The red profile was taken along a writing line, while the black was taken perpendicularly. The range of heights is the same for both directions. Apart from the peaks caused by writing lines, the perpendicular black profile changes much more sudden than the parallel red that has more continuous change overall.

Chapter 7

Results on multi-layer grating structures

The ultimate goal of the characterisation of optical effects in simple 3D-printing structures is to use the things we learned to create a more interesting structure. One of the steps that needs to be taken before more interesting structures can be attempted is to print in 3D.

The main focus in this research was on lattice-like structures, and thus the attempted 3D-structures consist of similar 2μm gratings as before, but now stacked on top of each other. Two samples are constructed from 2 stacked gratings. One has the second layer turned 90° as a simplest stacking choice. The other makes a 30° angle as to see how well the twisted part would go. For the 30° sample, the writing lines are actually not parallel with the bars in the second layer. This causes a discretisation effect not in height but bar shape, unlike the tilted planes which were discrete in the height. From looking at the optical images only, it is not clear if the areas under the overhanging bars are actually empty as they should be by design. With the 30° there is a division between two areas of the sample in how they scatter light from the imaging. It remains unclear how the physical structure are different, but the division of the structure in two areas hints at the involvement of the substrate finding problem, as with the divided gas bubbles from the one-layer gratings.

The third and last multi-layer sample is an attempt at a normal woodpile structure. This sample consists of two woodpile unit cells in the vertical direction. Together with the buffer flat plane at the bottom, this structure is build up of 9 layers. This sample took more than 100 hours to print.

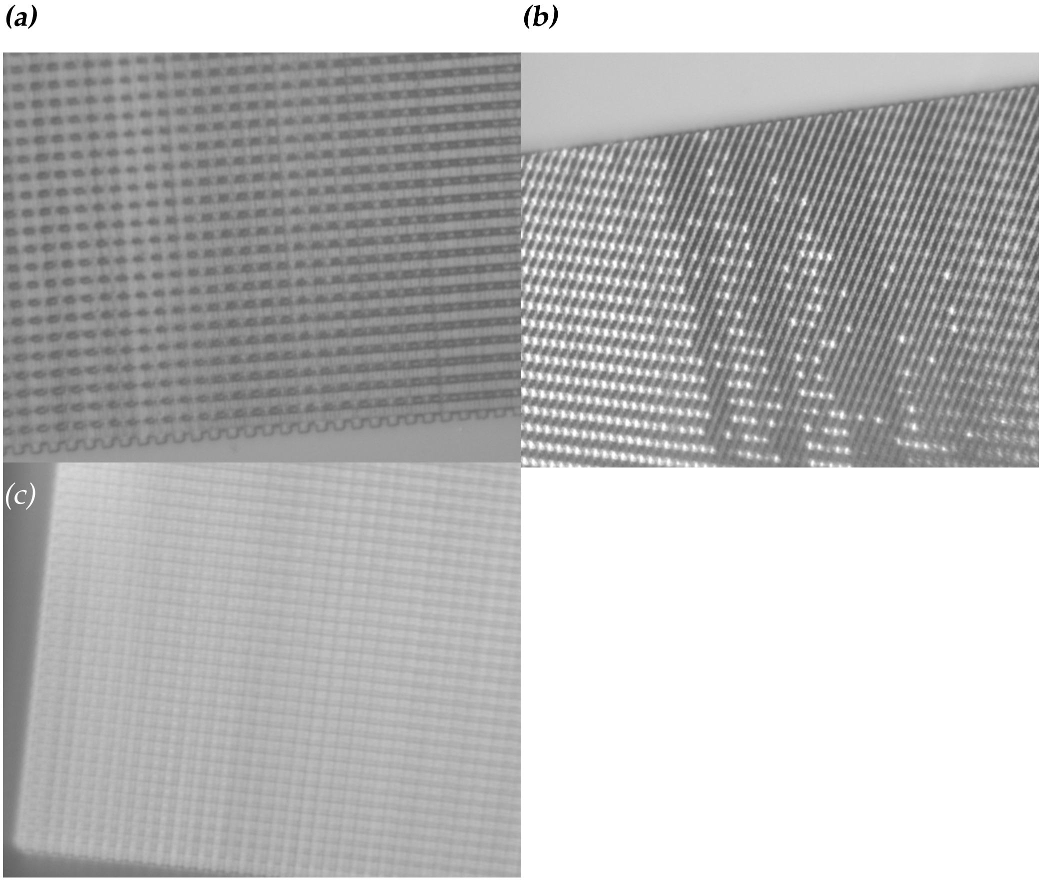

Figure 7.1: Optical microscope images of 3D-printed multi-layer gratings.
(a) shows the 2-stacked gratings on 90°. The two layers are individually visible., however at some parts they seem to be fused together as one thick layer. (b) shows the 2-stacked gratings on 30°. The top layer is visible, but the layer below, which should be vertical in this image, is not readily visible. The 30° were written with horizontal lines, resulting in discretisation of the bar on an angle. This is visible here as periodically squiggly bars. Half the sample has a different structure, which appears in this images as more light. The left side seems to have small blobs of material on the places of connection between the two grating layers. A divide like this is reminiscent of the writing laser mistakes in samples with a gradient caused by the Nanoscribe not finding the substrate surface, as in figure 5.1d. (c) shows the sample with two layers of woodpile, each 4 grating layers. Because of the depth, only one layer can be in focus. For this image it can only be concluded the bars have been printed at their proper location.

7.1 Transmission

As can be seen in figure 7.2, the far-field transmission patterns of the two-stacked-gratings samples are like a lattice of diffraction orders, but then projected on a sphere screen. Because of this, orders are along a curved line when projected on a flat screen. For the 90° structure, the two lattice vectors that make up the directions of the diffraction order lattice are perpendicular, as the grating bars are. The lattice vectors of the 30° structure are in a same way also 30° apart in direction.

The hypothesis about these stacked grating suggests the two grating layers diffract the light independently and therefore the second grating layer would just diffract every diffraction order of the first layer. This would then result in a decay in order intensity along any lattice vector line that is normal for a grating, which is inversely squared. However, in the intensity graph in figure 7.4 can be seen this not at all the case. In fact, even some second orders have significant power, which is atypical of square bar gratings. In both the 90° and 30° samples there is a extra bright diffraction order line through the zeroth order following the lattice vector corresponding with the second grating layer on the sample. This suggests the intensity distribution is biased towards the latest grating on the stack.

Apart from the lattice diffraction order structure, the blob line is also present in the stacked grating samples. In one direction do the orders seem to be connected by lines of scattered light blobs, see figure 7.2d for a detail of the blob line. For both 90° and 30° the scatter lines are in the same direction as the blob line that would be cast by a single grating that is aligned with the bottom grating layer of the stacked sample. This means the main source of the blob line is probably originating more from the bottom grating layer than the top one.

In the other direction between orders something else is going on. Neat vertical diffraction lines are visible in the horizontal direction departing from all diffraction orders, although weaker in intensity for weaker diffraction orders. These are also in the horizontal direction for the 30° sample. Close-ups of diffraction orders can be seen in figure 7.3. The periodicity of these diffraction lines corresponds with the diffraction pattern from a square aperture the size of the whole sample. Thus the explanation for these would be that the finite sample size also causes a diffraction pattern. This explanation also fits the horizontal direction in the 30° because the square sample is orientated in the same way.

The woodpile also has a square diffraction order lattice, similar to the 90° stacked grating. However,the diffraction orders are more faint and smeared out like stains. The zeroth order is way brighter in contrast. The stain-like diffraction orders suggest an imperfect alignment of all parallel grating layers, which would result in a slight spread in diffraction order angles. The blob line between the orders did not loose any intensity compared to the two stacked gratings samples, so they are relatively bright for this sample. The blob line is more of a band in this sample as it broadened together with the stain shape of orders.

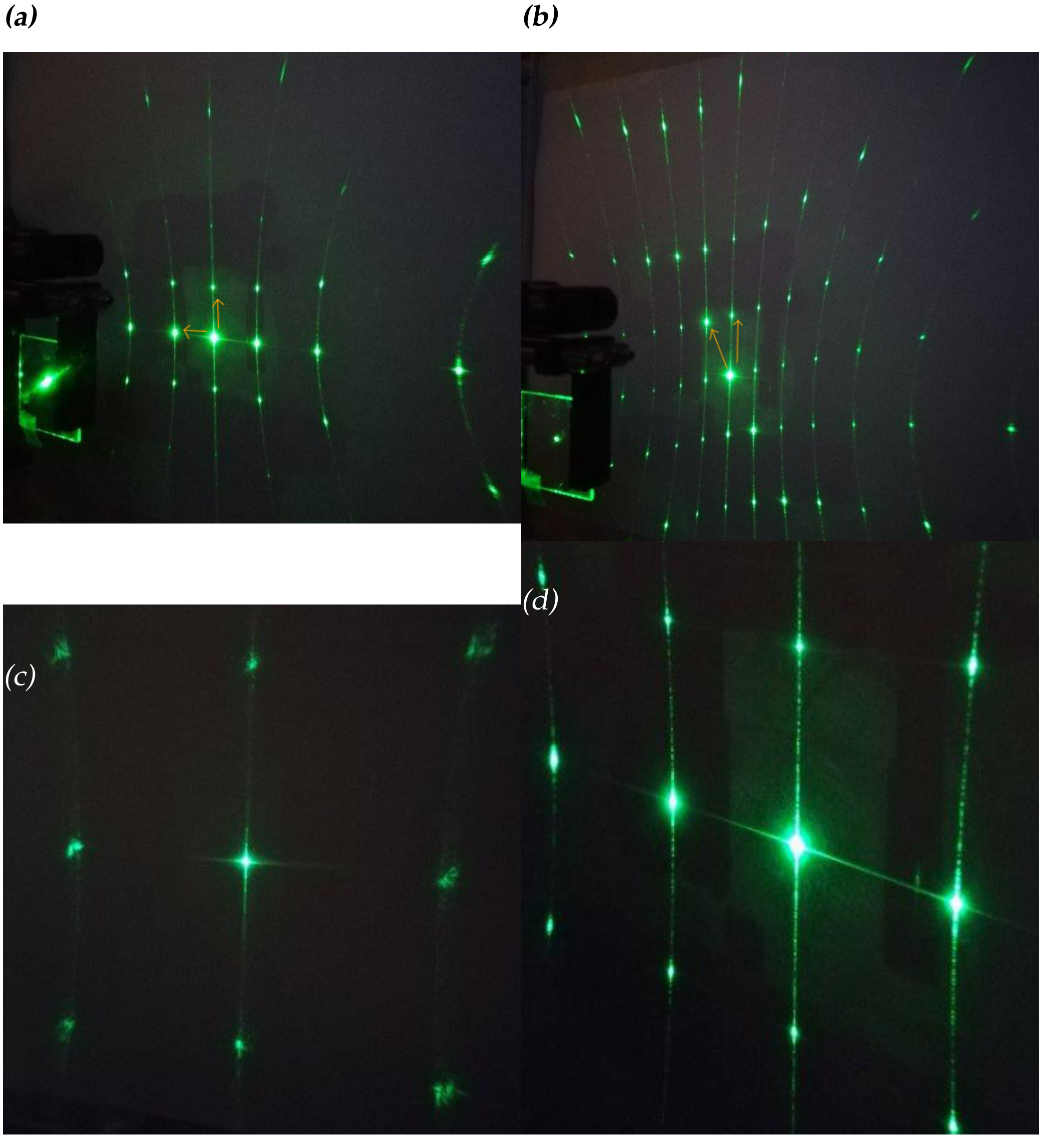

Figure 7.2: Transmission patterns of 3D-printed multi-layered gratings
The patterns of multi-layer gratings consist of diffraction orders in a lattice in k. Width and angle are related as in relation (2.2). This causes the lattice to look like as if projected from a sphere to a flat plane, widening at larger orders. The lattice vectors are determined by the orientation of the different grating layers. Just as in a single layer grating, the order direction is perpendicular to the direction of the bars in a grating layer. These lattice vectors are shown in orange. (a) is the transmission pattern from the 90° stacked grating, and thus the lattice vectors are also 90° apart. The sample on the substrate is visible on the left. The horizontal line through the zeroth order has the brightest orders. This direction corresponds with the top grating layer. Surprisingly, the even orders are visible very well in the horizontal direction. (b) shows the pattern of the 30° sample. The brightest orders are again in the direction corresponding with the upper grating layer, which is orientated 30° left from the vertical. The distribution of intensity seems to be more equal than a normal grating. (c) shows the pattern through the woodpile. It is a square lattice as well, but with most of the intensity focused in the zeroth order. The diffraction orders look like stains (not Gaussian) and are very broad, suggesting displacement between different parallel grating layers. (d) is a detail of the 90° pattern in (a). The blob line is only in the vertical direction and relatively bright for all multi-layer samples. For the woodpile the blob line is as broad as the stain-shaped orders.

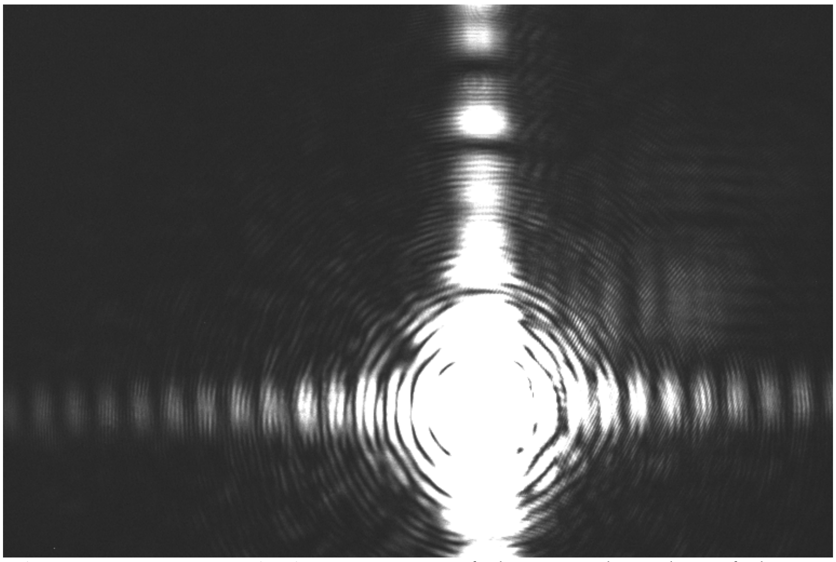

Figure 7.3: Transmission pattern of the zeroth order of the 90° 2-stacked gratings sample

Taken with the CCD camera. The horizontal line has regular diffraction lines. The periodicity of these lines match the square 250x250μm size of the sample. The vertical line is the blob line. There is no clear periodicity, but the source is presumably a long range periodicity from voxels by displacement, or long range structural periodicity in height. Matching with the blob lines in single layer gratings, the direction of this blob line aligns with the lowest printed grating layer. In the 30° sample, the pattern lines is also horizontal and vertical. This supports that the blob line originates from the bottom grating layer, which is aligned in the same way, and supports that the square sample shape is responsible for the horizontal line, because nothing else in that sample is in a direction for a pattern in horizontal direction.

***(a)** Stacked 90°* ***(b)** Stacked 30°*

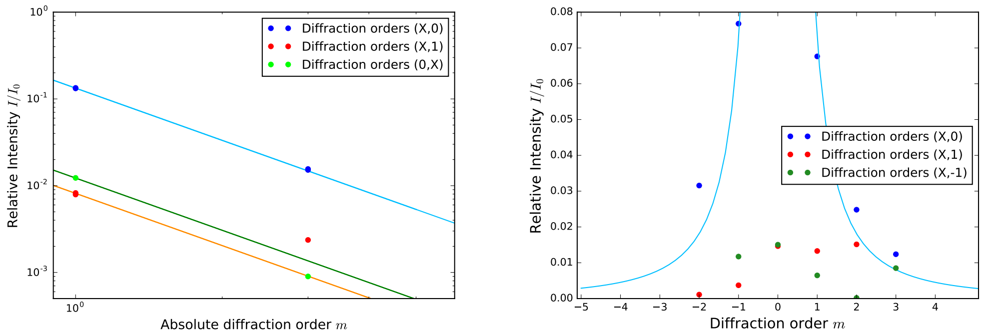

Figure 7.4: Intensities of diffraction orders in the transmission pattern of 2 stacked gratings.
These intensity measurements were done to check whether the two grating layers act independently on the light, as theorised in section 2.4. If this were the case, the intensity would fall off inversely squared with the order along any diffraction order lattice vector. Lattice locations are noted as (X,Y), where X is the lattice vector direction corresponding to the top layer in the stacked grating which are at 90° and 30° from the vertical for (a) and (b) respectively. Y represents the vertical direction. Lines of orders are noted with one coordinate kept as a variable.
In (a) are the intensities in lines plotted in loglog and fitted with inverse square fits. Only the brightest order line (X,0) in blue acts like as originating from a single layer grating. Lines parallel to (X,0), like (X,1) decay slower with higher orders, while those parallel lines as a whole decay faster in intensity as shown in (0,X) in green. For the 30° stacked grating in (a), the lines do not at all act inversely squared. As shown in blue, the brightest (X,0) decays slower. The (X,1) and (X,-1) lines mirror each other in intensity, but not itself in positive and negative order.
The model doesn't fit along all lattice vectors, and the both stacked grating samples can not be considered as two gratings acting independently.

7.2 Spectrometry

The woodpile structure is meant to act as a photonic crystal and should have a band gap. While only two layers of woodpile would not result in a perfect band structure as the theory of photonic crystals predicts, there might be some band structure resembling the homogeneous woodpile limit visible for this sample.

The measured band structure can be found in figure 7.5. While the expected band gap was expected to be imperfect and fairly weak, both because of the low amount of woodpile layers and the imperfections in 3D-printing, there is no real resemblance to a woodpile band structure with a gap found in this sample.

A physical explanation for the lack of visible band gap in this sample would be that it is printed directly on a substrate. In transmission through a finite photonic crystals, the effects of the band structure are reduced when the incident light comes from a material with a higher refraction index than the photonic crystal itself.[4] The printing material of the woodpile has a similar refractive index as the silica substrate, but half the sample's volume is actually air. This reduces the effective refractive index of the woodpile sample and results in a less profound band structure.

In order to improve the sample as to have a visible woodpile band structure, the sample could be printed on a few pillars instead of directly on the substrate. This would create a volume of air with low refraction index as the incident light medium and alleviate the problem stated earlier.

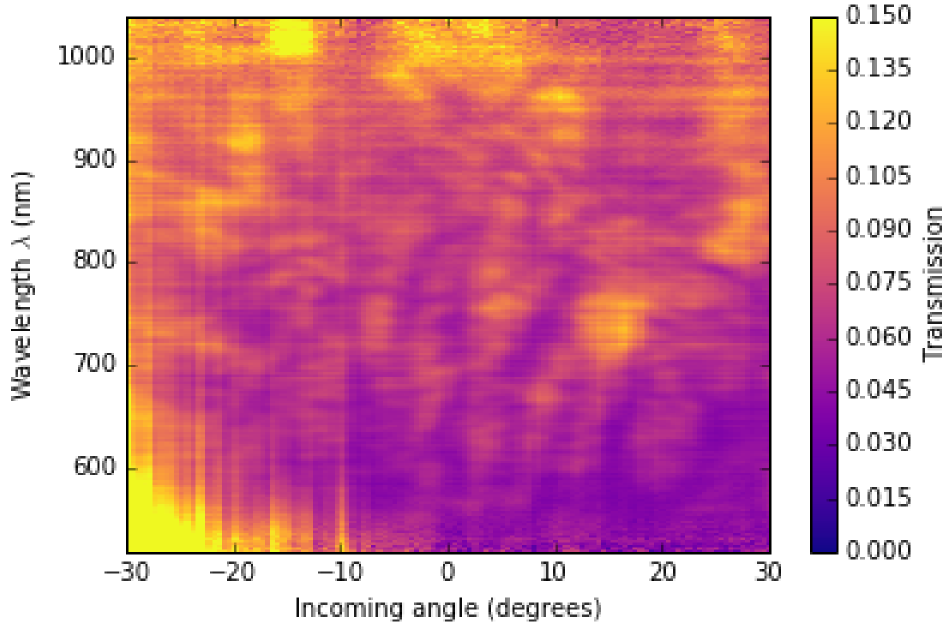

Figure 7.5: Transmission spectrum of the zeroth order of 2-layer woodpile structure at different incident light angles.
This could be interpreted as an optical band structure, with the wavelength equivalent to energy and the incident angle as a form of varying a k-vector. However, no band is found in this spectrometry figure. The low transmission does not seem to correspond with the laser transmission setup, which showed more than half of the intensity in the zeroth order, at 520 nm (not shown in this figure). However, the intensity rises at the lower wavelengths. The more probable answer is that the sample wasn't aligned properly in height, which was hard to do in the spectrometry setup. This does not undermine the result, as the band structure should still be visible.

Chapter 8

Conclusions

8.1 Suggestions on the production process

It became apparent from the AFM images of the gratings that the resemblance of produced structures to the intended structures decreased dramatically with grating features smaller than 2 μm. The main reason for this was the egg like voxel shape together with displacement which made it hard to create sharp corners and maintain the right thickness of the bars. This problem got enhanced because of the use of multiple writing lines for one feature.

One future solution for this is to avoid features smaller than 2 micron in the structure, and stick to single writing line features if needed for smaller features. This does increase the wavelengths for which interesting structures can be made.

Another option is to improve the writing at smaller scales by employing the full scale of the possibilities of the Nanoscribe. The voxel size can still be decreased by reducing the writing laser power. However, similar as with the one-photon polymerisation, this makes the voxel shape vulnerable to small variations in laser power which can be caused by the writing environment as well. There has been experimenting with this production method in this research.

Another option which has not been experimented with is the possibility to write continuously along any line path through 3D space. This would be very important when creating structures which do not mainly consist of straight lines, for example optical lenses. The tilted plane samples could have been produced with lines following the gradient instead.

The parameter which was hardest to control turned out to be the height. The main problem with the 4 μm sample was the difficulty of the Nanoscribe to find the surface. The buffer plane solution has not been proven to work, because AFM image of the gap of the smaller samples were inconclusive and did not result in height measurements.

From the flat plane it was apparent there was some form of displacement in height that varied with location on a length scale of a few micron. These might be the cause of the blob line, but the physical reason of these height variations is unclear. In order to create better optical sample, without the blob line, this has to be resolved.

The need in optics for filled 3D structures instead of mechanical shapes that can be left empty takes up a lot of writing time. Reductions in writing time are possible. For example by moving the writing laser continuously, also when it is turned off, and not stop it every time it switches on and off. This is the standard choice, as to not have the transition between on and off affect the structure. However it might not have been needed with the large gaps between the grating bars. If it does turn out to have an effect on the structure, the sample can still be improved for multi-layer samples by writing every grating layer parallel with the bars. This avoids the discretised diagonal bars in the 30°sample.

While the 250x250 μm sample size was somewhat arbitrary, the choice was made to create a macro-sized sample. The most obvious choice of reducing writing time is to reduce the sample size. Furthermore, if the sample size is smaller than 100 μm another writing technique of the Nanoscribe can be used. This method relies on aiming the laser with a galvo mirror system and is very much faster.

The experiments on the tilted plane samples demonstrated it was not fit to act as a smooth surface, with the sample acting truly as a grating with diffraction orders and not as a wedges with one refracted beam. This shows the step to 3D-printing lenses is more difficult than anticipated. The solution to smooth surfaces could be sought for in the Nanoscribe's abilities. However, post-curing methods have been proven to be effective in the 3D-printing production of lenses.[15] Using post-curing methods could be the direction to take to improve samples with smooth surfaces.

8.2 Comparison of different characterisation methods

In this project, we have been able to connect most of the optics that was seen in single-layer structures to properties of the structure. The transmission setup mainly provided the means to investigate the optical effects of displacement and variation in duty-cycle. The expected effects were observed in a quantitative way, in width and intensities of diffraction orders, and the causes were confirmed with the AFM images. However, optical effects have not been quantitatively linked with the structural properties of the sample. The missing link is the missing quantitative characterisation of the relevant structure properties, while this might have been possible with the data collected. Nonetheless, the transmission setup has been successful in its goal for single-layer samples. For multi-layer sample, like the woodpile structure, it has only been useful as a qualitative tool to confirm the misalignment of parallel layers, which did not give any new insight.

The spectrometry setup had useful results. The model worked as a means of measuring the height for a single-layer grating. Even if there was not one well defined height, this method worked with an effective height. The spectrometry results also gave insight in height related flaws like a gradient in height. Because of setup's potential as a device to measure a band structure, it will be the characterisation method of choice for multi-grating layer structures.

The AFM imaging was instrumental in observing the actual structure of the sample and should be used for any 3D-printed acrylic structure of this scale. The individual writing lines were imaged and their shape was visible. This is the highest resolution that is needed to characterise the structure. The AFM has been able to show most of the possible flaws that the 3D printer could make that had relevant optics attached: Displacement by imperfections, variation of duty-cycle, surface roughness from both writing lines and imperfections, and even the surface finding problem.

The AFM imagery was unable to image the gaps between bars reliably. This leaded to unreliable height measurements of the bars and resulted in doubts about the rectangular shape of the bars.

The AFM did show long range periodicity in the flat plane, it did not show this in the grating samples. Non of the optical methods have been successful in quantitatively characterising the blob line. As it has been qualitatively observed this becomes more prevailing with the multi-layer samples, it might be necessary to investigate it with another method.

8.3 Outlook on future 3D-printed structures for optics

With the exploration of 3D-printing in one layer gratings done in this research, future research should focus more on stacking the gratings. This project has done little to understand how the layers are attached and what the optical effect of this is. Furthermore, efforts to produce a woodpile with characteristic band gap have failed, without an explanation why, except some proof for misalignment of parallel layers by displacement imperfections.

Other research efforts should be aimed towards understanding the blob scattering, which was present in transmission of all 3D-printed samples. One proposed experiment which could shed light on the problem is to print a grating with the writing lines perpendicular to the bars, in order to investigate the source of the irregular blob line.

When these problems are resolved, the end goal of researching a twisted woodpile, or multi-layer grating structure, can be achieved.

Chapter 9

Acknowledgements

I want to express my gratitude to the following people, whom without this bachelor project would not have been realised.

Jeroen Mesman, for operating the Nanoscribe machine.

Daniëlle van Klink & Michiel de Dood, for the use of their spectrometry setup.

Erik de Vos & Federica Galli, for their help with the AFM imaging.

Martin van Exter, who was the supervisor for this project.

Bibliography

[1] S. John, *Strong localization of photons in certain disordered dielectric superlattices*, Phys. Rev. Lett. **58**, 2486 (1987).

[2] K. E. Drexler, *Engines of creation*, Anchor Press/Doubleday, 1986.

[3] J. J. D. Joannopoulos, S. Johnson, J. N. J. Winn, and R. R. D. Meade, *Photonic crystals: molding the flow of light*, Princeton University Press, second edition, 2008.

[4] E. Driessen, *Coupling light to periodic nanostructures*, Leiden University, 2009.

[5] *Nanoscribe website homepage*, `https://www.nanoscribe.de/en/`, Accessed: 2018-03-04.

[6] S. Y. Lin, J. G. Fleming, D. L. Hetherington, B. K. Smith, R. Biswas, K. M. Ho, M. M. Sigalas, W. Zubrzycki, S. R. Kurtz, J. Bur, and J. J., *A three-dimensional photonic crystal operating at infrared wavelengths*, Nature **394**, 251 (1998).

[7] H.-B. Sun, Y. Xu, S. Juodkazis, K. Sun, M. Watanabe, S. Matsuo, H. Misawa, and J. Nishii, *Arbitrary-lattice photonic crystals created by multiphoton microfabrication*, Opt. Lett. **26**, 325 (2001).

[8] Q. Sun, S. Juodkazis, N. Murazawa, V. Mizeikis, and H. Misawa, *Freestanding and movable photonic microstructures fabricated by photopolymerization with femtosecond laser pulses*, Journal of Micromechanics and Microengineering **20**, 035004 (2010).

[9] L. Maigyte, V. Purlys, J. Trull, M. Peckus, C. Cojocaru, D. Gailevičius, M. Malinauskas, and K. Staliunas, *Flat lensing in the visible frequency range by woodpile photonic crystals*, Opt. Lett. **38**, 2376 (2013).

[10] M. Thiel, G. von Freymann, and M. Wegener, *Layer-by-layer three-dimensional chiral photonic crystals*, Opt. Lett. **32**, 2547 (2007).

[11] N. Muller, J. Haberko, C. Marichy, and F. Scheffold, *Silicon hyperuniform disordered photonic materials with a pronounced gap in the shortwave infrared*, Advanced Optical Materials **2**, 115 (2014).

[12] E. Hecht and A. Zajac, *Optics*, Addison-Wesley Publishing Company, Inc., 1974.

[13] *Basel problem - Wikipedia*.

[14] *M squared, beam quality factor - Wikipedia*.

[15] X. Chen, W. Liu, B. Dong, J. Lee, H. O. T. Ware, H. F. Zhang, and C. Sun, *High-Speed 3D Printing of Millimeter-Size Customized Aspheric Imaging Lenses with Sub 7 nm Surface Roughness*, Advanced Materials **1705683**, 1705683 (2018).